AN EXPERIMENTAL STUDY OF SMALL PORE ZEOLITES FOR THE UPGRADING OF BIOMASS TO FURFURAL

by

Spencer Michael Bruce

A thesis submitted in partial fulfillment
of the requirements for the degree

of

Master of Science

in

Chemical Engineering

MONTANA STATE UNIVERSITY
Bozeman, Montana

August 2015

TABLE OF CONTENTS

TABLE OF CONTENTS - CONTINUED

LIST OF TABLES

LIST OF FIGURES

Figure Page

LIST OF FIGURES - CONTINUED

Figure Page

LIST OF FIGURES - CONTINUED

Figure Page

ABSTRACT

Furfural derived from lignocellulosic biomass is a valuable platform molecule in the production of renewable liquid fuels and chemicals. With ever-increasing emphasis on reducing dependence on traditional petroleum-derived fuels and chemicals, the production of value-added chemicals from biomass has the potential to have a major global economic and environmental impact. To do so efficiently and sustainably requires the development and evaluation of new catalysts for these applications. These catalysts must not only be effective at catalyzing the conversion of sugars to furfural, but also must be easily separated, regenerated, and reused following each reaction.

In this study, several small pore zeolites and metal-organic frameworks (MOFs) were evaluated for use in the dehydration of xylose, glucose, and switchgrass to furfural in a monophasic system of 90/10 γ-valerolactone (GVL)/water. Based on results of initial experiments, three small pore zeolites, SAPO-34, SAPO-56, and DNL-6, became the major focus of these studies. The pore sizes of these molecules are significantly smaller than the kinetic diameters of xylose and glucose, which would lead one to predict minimal furfural production over these catalysts due to limited acid site access. In spite of that, moderate furfural yields of approximately 40% were achieved over SAPO-34 and SAPO-56 from xylose. Moderate furfural yields were also achieved from non-pretreated switchgrass over the SAPO catalysts in the GVL/water system, with strong evidence that both xylose and glucose were converting to furfural. Furfural degradation in GVL/water was minimal compared to degradation in a purely aqueous solvent. No leaching of acid sites occurred with the SAPO-34 catalyst, and it was recycled multiple times with only a 5% drop in furfural yield from first to final reaction. Most previous research using zeolite catalysts to upgrade biomass has focused on medium and large pore zeolites, as their pore apertures more closely match the kinetic diameters of the relevant component sugars of biomass. The results presented in this study suggest that small pore zeolites are also worthy of ongoing research.

1.0 INTRODUCTION

1.1 Background

Petroleum-derived energy, fuels, chemicals, and materials are a ubiquitous part of modern society. On top of providing the primary source of liquid fuel for most of today's vehicles and electricity for many residences and businesses, other petroleum-derived products are also pervasive across all areas of our lives. A significant amount of the clothing we wear, the products we use around the home or office, the streets we drive our vehicles and ride our bicycles upon, and our homes themselves are comprised of substantial quantities of products derived from crude oil.

While current domestic production of crude oil and natural gas are both at all-time highs,[1] disasters like BP's 2010 Deepwater Horizon oil spill in the Gulf of Mexico[2] and recent reports linking wastewater injection from hydraulic fracturing ("fracking") to an increase in localized earthquakes in historically inactive seismic regions[3-5] are motivating tighter regulations and policy changes within the industry. Recent incidents like these seem to also be causing a slow paradigm shift within the general public, leading to a growing acceptance of anthropogenic climate change[6] and the urgent need to look toward alternative sources of energy and raw materials for manufacturing industries. This trend, coupled with a growing demand for crude oil in rapidly developing nations like India and China, highlights an increasingly urgent need for innovation and advancement in this space.

1.2 Biomass Overview

The amount of plant biomass harvested annually worldwide is estimated to exceed 1.8 trillion tons, of which almost 95% is lignocellulosic biomass.[7-8] In the United States alone, 1.4 billion tons of biomass can be produced sustainably every year.[9] Lignocellulosic biomass is generally inedible for humans, making it an excellent candidate from which to derive important chemicals and fuels. With recent estimates by the United Nations of over 805 million undernourished people (11% of the global population) throughout the world,[10] the importance of developing processes to produce renewable chemicals and fuels from inedible lignocellulosic biomass, rather than from edible plants and plant components, has never been more imperative. While lignocellulosic biomass is an attractive source of renewable material, its implementation and use in chemical processes is complicated because of its complex and varying composition.[11]

1.2.1 Components of Biomass

Biomass is primarily made up of three primary components: cellulose (38-50%), hemicellulose (23-32%), and lignin (15-25%).[12] Cellulose (Figure 1) is a rigid polymer typically composed of 7,000 to 15,000 individual glucose units.[13] It is difficult to hydrolyze due to significant hydrogen bonding, but it has seen a substantial increase in interdisciplinary research over the past 20 years, and already sees significant use in industry as a polymeric raw material source for many different products.[14]

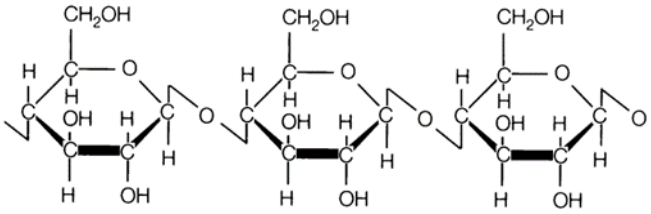

Figure 1: Typical structure of cellulose.

Hemicellulose (Figure 2) is typically a branched polymer, consisting of 500 to 3,000 monomer units.[13] It is easily hydrolyzed to xylose and other C_5 sugars, but is more complex than cellulose in that it contains many different sugar monomers, whereas cellulose typically only contains glucose.[15] Xylose is commonly the most abundant sugar monomer, but hemicellulose also typically contains smaller amounts of mannose, arabinose, galactose, rhamnose, glucose, and others.

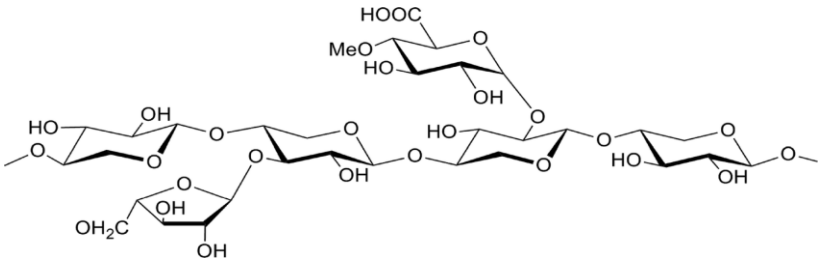

Figure 2: Typical structure of hemicellulose.

Lignin (Figure 3) is a highly variable aromatic polymer and is the second most abundant polymer found in nature.[16] The precise composition of lignin varies tremendously from species to species, but currently sees industrial use as a good raw material for some applications, such as production of polyurethane, polycarbonates, and asphalt, and a source of energy in the pulp and paper industry.

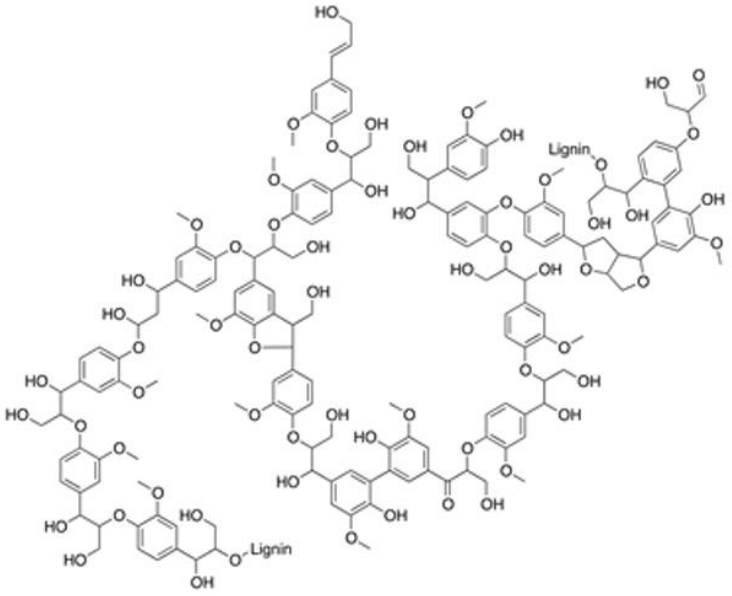

Figure 3: Typical structure of lignin.

1.2.2 Furfural: An Important Platform Chemical Derived from Biomass

Among the chemicals that can be produced from lignocellulosic biomass, furfural, is of particular interest. Furfural (Figure 4) has the potential to replace petroleum-based organics in the production of lubricants, adhesives, and plastics as well as act as a direct additive to fuel blends.[17-19]

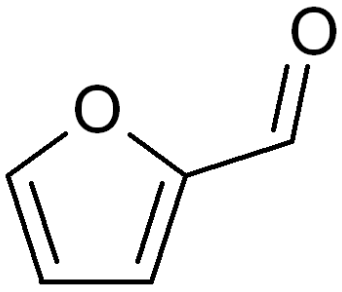

Figure 4: Structure of furfural.

It is most easily produced via a simple dehydration reaction from xylose (Figure 5),[20] the primary monomeric component of hemicellulose. Glucose also is capable of converting to furfural, but must do so via a less favorable reaction mechanism (Figure 5).[19]

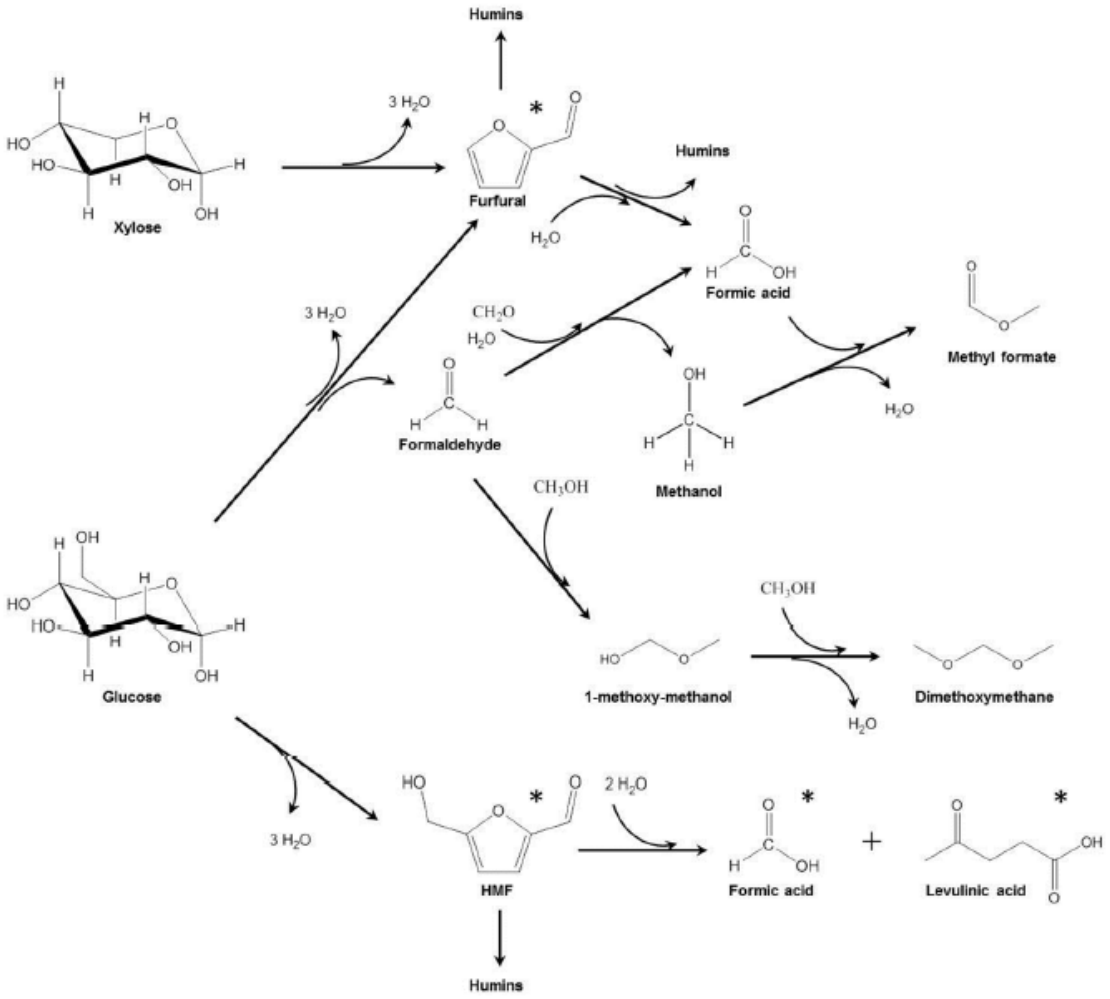

Figure 5: Proposed reaction pathways for dehydration of xylose and glucose to furfural.

Furfural is a renewable chemical feedstock that is important in many processes today. As early as 1939, furfural saw significant use as a preservative, fungicide, herbicide, disinfectant, and production of phenolic resins, maleic acid, and many other chemicals.[21] Today, most furfural is converted via hydrogenation to furfuryl alcohol,

which is an important chemical used in the manufacture of many polymers and plastics.[22] Other compounds derived from furfural include methylfuran and tetrahydrofuran, which are also important platform chemicals in the production of many other polymeric chemicals and products. Furfural and its derivatives are also used today as a replacement for petroleum-derived organics in the production of various lubricants and adhesives.[23] Furfural can also serve as a building block for potential transportation fuels and fuel additives, such as dimethylfuran and ethyl levulinate. Lange et al,[18] among others,[24] provide excellent reviews of the many proven catalytic processes to synthesize furfural, as well as the many uses of furfural as a fuel additive and as a platform chemical for other value-added chemicals.

Furfural was initially isolated in 1821 by a German chemist, Johann Wolfgang Döbereiner, as a byproduct from the synthesis of formic acid.[22] Furfural was not produced industrially until 100 years later, when in 1921, the Quaker Oats Company began producing furfural from leftover oat hulls using abandoned 8 by 12 foot iron pressure cookers in their Cedar Rapids, Iowa, USA facility.[25] Today, furfural is still produced via the batch process first developed by Quaker Oats in 1921. A similar batch process is used throughout China, which achieves a furfural yield of approximately 50%.[25] Continuous processes have also been developed and used by Quaker Oats (now abandoned), Escher Wyss (also now abandoned), and Rosenlew.[25] Several modern day process are currently in the pilot plant stage, and show major potential to enhance and improve the way that furfural is produced. Table *1* below gives a brief overview of some

common furfural production process, both past and present. Some data and operating conditions for these process are still proprietary and not available to the public.

Over the first decade of the 21st century, furfural prices have ranged from $650/ton to $1200/ton. China currently houses approximately 80% of the world's furfural production capacity, and consumes approximately 75% of what is produced globally. Because of this, global furfural prices are determined largely by domestic issues in China, making prices difficult to predict. Prices are expected to remain in the $1400/ton to $1500/ton in the immediate future.[26] As such, the development of more efficient and sustainable furfural production processes has been and will continue to be an important area of academic and industrial research.

Table 1: Current industrial scale furfural production processes (adapted from Montastruc et al[27]).

	Batch Process	**Quaker Oats**	**Supratherm**	**Vedernikov**
Temperature (°C)	140-180	--	200-240	--
Pressure (atm)	6	10	20-30	--
Residence Time (hrs)	5	1	<<1	--
Yield (%)	50	55	70	75
Status	Commercialized	Commercialized	Pilot Plant	Pilot Plant

1.2.3 Switchgrass as a Source of Biomass

Nearly 35 years ago, it was recognized that dedicated bioenergy feedstock crops would become an important part of the United States' renewable energy strategy, which led to the initiation of the Bioenergy Feedstock Development Program (BFDP) at Oak Ridge National Laboratory in 1978 by the US Department of Energy.[28] In the early

1990s, the "BFDP recognized that expanded emphasis was needed on the development of herbaceous bioenergy crops that could combine close compatibility of crop management strategies with existing farming practices, generate cash flow from annual returns from harvested biomass, and have positive environmental impacts on American farmlands."[29] This led to a major effort to evaluate and develop Switchgrass as a potential bioenergy feedstock crop.

Switchgrass (*Panicum virgatum*) is an extremely hardy and adaptable plant that grows well in many diverse climates, including the dry prairies of Montana. Switchgrass has been shown to be a highly productive crop across a wide geographic range and in areas of marginal quality land, with limited nutrients and low water.[30] It has also been shown to possess positive environmental attributes.[31] Due to its deep fibrous root system and high growth heights, it acts as a good preventative measure against soil erosion from wind and water, and has been used as such throughout the United States.[32]

While switchgrass is an intriguing feedstock crop due to its growth attributes and tangential environmental benefits, its chemical composition also makes it an ideal feedstock crop for sustainable production of biofuels and chemicals. On a dry matter basis, switchgrass contains approximately 37% cellulose, 29% hemicellulose, and 19% lignin, although this can vary based on specific growing conditions, geography, and other factors.[33] Switchgrass was chosen to be the focus of these studies due to the reasons outlined above, and also due its already common growth in this region (Northern Rocky Mountains & Plains) and easy access to uniform and representative samples from Dr.

Brett Allen at the US Department of Agriculture's Northern Plains Agricultural Research Laboratory in nearby Sidney, Montana, USA.

1.3 Current State of Research on Biomass Upgrading

Research into the transformation of various plant species and components of biomass into renewable fuels and chemicals is currently a major interest area across academia, industry, and government research labs. In order to make better sense out of the many different directions this research can take, many people often discuss renewable fuels and chemicals in terms of generations.

1.3.1 First Generation Biofuels & Chemicals

First generation biofuels utilize various vegetable oils and corn to produce biodiesel and bio-ethanol. Biodiesel is produced commercially via a fairly simple transesterification reaction, typically using waste vegetable oil from restaurants as a feedstock. Biodiesel offers several advantages over petroleum-based diesel fuel in terms of common issues with the lubricity and cetane index of petro-diesel, but production cost is a major obstacle to a massive scale-up and adaptation of biodiesel in place of petro-diesel.[34] It is currently most often used in the US in blends between 1% and 20% with petro-diesel, and is limited in part by its compatibility with modern diesel engines. Bio-ethanol is most often produced from corn in the US. Studies have shown that while corn-based bio-ethanol is less petroleum-intensive than gasoline, it has greenhouse gas emissions similar to those produced from gasoline.[35] Corn-based ethanol also relies heavily on government subsidy in the US to remain economically viable. Ethanol

produced from sugarcane, though not a reasonable feedstock alternative in most US, has been shown to achieve double the greenhouse gas emissions reduction per unit of harvested land versus that of corn ethanol and is much more economically feasible due to sugarcane's higher energy content.[36] While there is currently a significant amount of production capacity throughout the US of these first generation biofuels, there are also many concerns about impacts of first generation feedstock crops on biodiversity and competition with food crops.[37] That, coupled with their dubious environmental benefits and marginal profitability, have led to exploration of many other options for renewably produced biofuels and chemicals.

1.3.2 Second Generation Biofuels & Chemicals

This research focused on second generation feedstocks since they are produced from lignocellulosic biomass, non-edible plants and the non-edible parts of food crops, which circumvents the competition first generation biofuels face with food crops. Biorefineries attempt to utilize biomass for production of fuels and other chemicals, but significant innovation and advancement is needed before these biorefineries can operate profitably and in a way that provides major environmental advantages over other existing bio-products and petroleum products.[37-38]

1.3.3 Next Generation Biofuels & Chemicals

Many other approaches to biofuels and bio-products also exist today.[39-40] Among the most well-known are algal biofuels,[41] which are receiving a tremendous amount of research worldwide due largely to their non-competition with other crops and practically

limitless growth potential in the world's oceans. Other current approaches are more focused on better utilizing existing biomass feedstocks or engineering new next-generation biomass feedstocks.[42] Other researchers are currently working to develop ways to produce biomethane from waste and synthetic biofuels from the gasification of biomass.[43] All of these emerging technologies require substantial work before they are feasible on an industrial scale. One of the primary goals for all of these newer technologies is to avoid some of the environmental issues and eventually, the economic issues facing currently available technologies.[40]

1.4 Lignocellulosic Biomass Conversion Strategies

A significant body of research investigating the conversion of cellulose and hemicellulose into chemicals has focused primarily on either enzymatic[44-47] or mineral acid catalysis.[48-49] While both of these methods are able to achieve some level of success, they also present a major issue for scale-up and commercialization: namely, separation of the catalyst from the reaction mixture and its subsequent reuse or recycling. Recently, it was found that using γ-valerolactone (GVL) as a solvent stabilizes furfural, which decreases degradation reactions,[19, 50] and also solubilizes corn stover and other lignocellulosic biomass,[19, 51] which allows for a simple filtration step to separate heterogeneous catalysts from the solution.[7, 19, 52-54]

Possible heterogeneous catalysts for the conversion of sugars to platform chemicals include micro- and mesoporous solid acid materials, such as ion-exchange resins and zeolites. Researchers have demonstrated that porous acid catalysts have the

potential to fill an interesting niche in sugar dehydration chemistry if their catalytically active sites can be stabilized. The potential shape selectivity of zeolites could lead to tailored, highly specific reactions. The three main types of porous catalysts studied for sugar dehydration reactions are: mesoporous silica, ion exchange resins, and medium pore size zeolites.

1.4.1 Mesoporous Silica Catalysts and Biomass

Mesoporous silica nanoparticles, such as MCM-41 and SBA-15 (Figure 6), are a class of molecules that have garnered significant attention since the mid-1990s due to their potential use in catalysis, separations, drug delivery, optical devices, and others.[55] Mesoporous silica was originally produced and patented in 1971,[56] but remained reasonably unknown and unpopular until it was produced via the same procedure again in 1997.[57] Various synthesis methods[58-60] and many applications and research interests with mesoporous silicas exist today.[61-62]

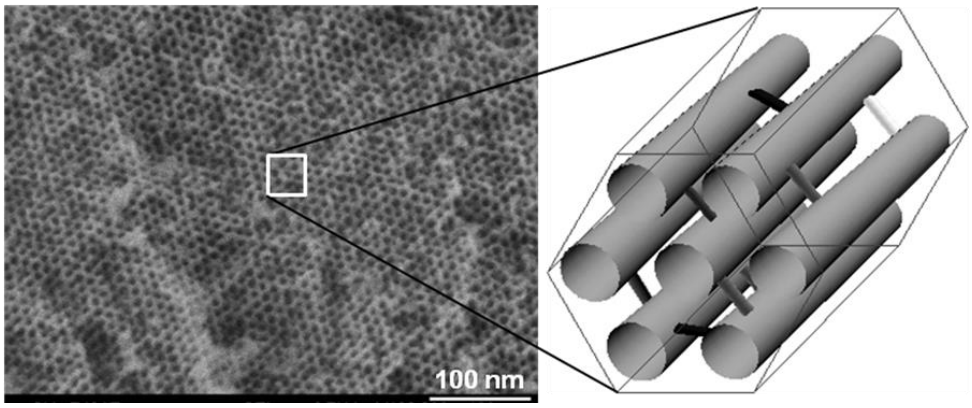

Figure 6: Representative image of SBA-15, a common mesoporous silica nanoparticle. (Adapted from Kleitz et al[63])

In biomass upgrading applications (specifically dehydration of xylose to furfural), mesoporous silicas have shown 40-70% furfural yield,[19, 64] minimum diffusion limitations, and the potential to tune acid sites (surface functionalization). Many of these catalysts undergo deactivation due to leaching and surface passivation, and are difficult to regenerate due their hydrothermal instability, making them less than ideal catalysts for xylose dehydration at present.[65-67]

1.4.2 Ion-Exchange Resin Catalysts and Biomass

Ion-exchange resins are a broad class of insoluble matrices created from an organic polymer substrate. They are most often found in the form of small porous beads, which means they have an extremely high surface area and are able to selectively trap some ions while simultaneously releasing other ions.[68] They have a high degree of structural variability and can be highly customized, leading to a variety of important uses such as: water softening and purification,[69] metal separation and purification,[70-71] catalysis,[72-73] and many other industries.

Ion-exchange resins have shown the highest yields to date along with minimum diffusion limitations, but their hydrothermal stability is limited, and leaching of acid sites into the solution can occur.[74-75]

1.4.3 Medium Pore Zeolite Catalysts and Biomass

Medium pore size zeolites with pore apertures in the 5-8 Å range are appealing candidates as they demonstrate a molecular sieving effect since sugar molecules have kinetic diameters in the range of ~6-9 Å with xylose being 6.8 Å[76-77] and glucose being

8.6 Å.[78] ZSM-5, one of the most studied and widely used medium pore zeolites today, has a uniform framework and pore apertures of 5.5 Å, as shown in Figure 7. Medium pore size zeolites have shown medium-to-high hydrothermal stability, are easy to regenerate, and can contain a high amount of Brønsted acid sites, which promote the conversion of xylose into furfural.[79-80]

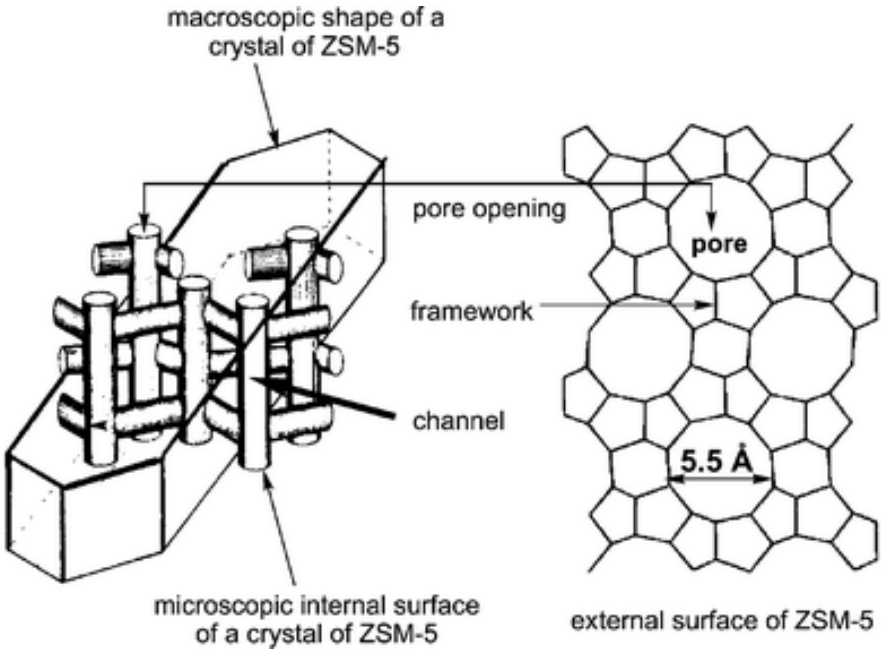

Figure 7: Structural framework details of ZSM-5, a common medium pore zeolite. (Adapted from Lei et al[81])

Due to all of the positive attributes of medium pore zeolites mentioned above, a variety of them have been studied as catalysts for the conversion of xylose to furfural. The highest reported yields were from mordenite, which resulted in a furfural yield of nearly 80% at 448 K in a 90/10 wt% GVL/water solvent.[19] In aqueous environments, however, mordenite and faujasite both resulted in high furfural selectivities (80–90%) at 443 K, but low yields (approximately 25%) due to decreased selectivity as the reactions

progressed.[82] Other zeolites, including H-beta,[19,83] Y,[84] ZSM-5,[19, 85] and H-zeolites,[86] have been used for xylose dehydration with varying yields (40-70%) of furfural and its derivatives, and silicoaluminophosphates (SAPO-11, SAPO-40, and SAPO-5) resulted in furfural yields of only 20-40%.[83] A significant amount of other data has been published relating to medium pore zeolites and xylose dehydration, but these examples give a pretty complete overview of the benefits, yields, and limitations associated with this class of catalyst.

1.5 Zeolites: A Deeper Look

Zeolites are microporous minerals composed of aluminum, silicon, and oxygen ("aluminosilicate") that have a wide range of commercial uses. They are used commercially as catalysts by the petrochemical industry, as adsorbents in laundry detergent and cat litter, and for various applications in the medical industry, among many other uses. They occur naturally in many conformations (Figure 8 and Figure 9), but these naturally occurring forms are not of much value industrially. This is because their chemical composition is non-uniform, they often contain impurities, and they are not naturally optimized for catalytic applications.[87] A turning point in the history of zeolites was the introduction of synthetic faujasites to the process of fluid catalytic cracking of heavy petroleum products by Milton et al in 1962.[87-88] Fluid catalytic cracking remains an enormously important and profitable aspect of the oil refining process to this day. This spurred a period of rapid development in the area of zeolite-catalyzed industrial processes, today accounting for the single largest application of zeolites in a financial

sense.[89] In order to be used industrially, synthetic zeolites are typically either formed into a uniform and useable shape (such as the pellets shown in Figure 10) or are crushed into a fine white powder.[90]

Figure 8: Gismondine is one example of a naturally occurring zeolite.[91]

Figure 9: Chabazite is another example of a naturally occurring zeolite.[92-93]

Figure 10: Synthetic zeolite pressed into pellets for industrial use.[94]

1.5.1 Structure and Function of Zeolites as Catalysts

The framework of a typical zeolite molecule is highly uniform and rigid, and contains many pores and channels of identical size. Zeolites are typically solid acids, and the density, strength, type, and location of acid sites of a zeolite varies widely from one type to another. Most zeolites are also highly stable under high temperatures, pressures, and extreme chemical environments. These properties, among others, make them exceptional catalysts across an enormous range of applications.

Most relevant to their catalytic capabilities is a discussion of the acidic properties of zeolites. In analyzing acidic properties of zeolites, several distinctions must be made, including: the nature of the acid sites (Brønsted vs. Lewis acidity), the density of the acid sites, the strength of the acid sites, and the precise location of the acid sites.[87]

The distinction between Brønsted (proton donor) and Lewis (electron pair acceptor) sites is an important one because these two types of acid sites are known to

affect the kinetics of a given reaction in completely different ways, and even to catalyze different reactions entirely under the same initial conditions.[20, 95-96] In the reaction of highest interest in this project, the dehydration of xylose to furfural, the varying roles of Brønsted and Lewis sites are summarized nicely by Choudhary et al[20] in Figure 11 below.

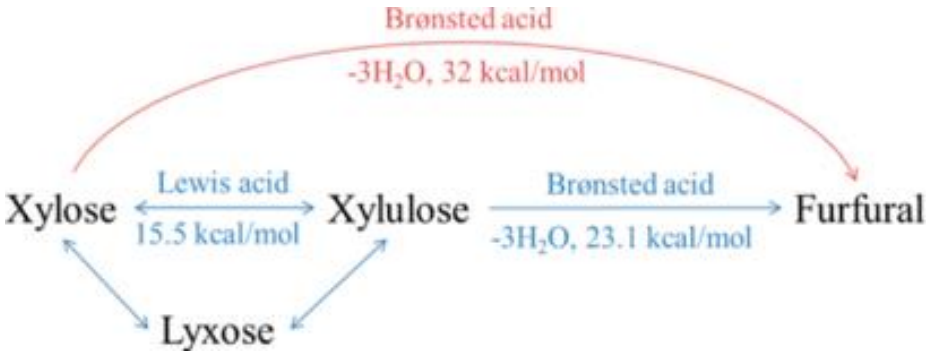

Figure 11: Competing roles of Brønsted and Lewis acid sites in the dehydration of xylose.[20]

A catalyst with a significant concentration of accessible Lewis and Brønsted acid sites would catalyze a xylose to xylulose conversion (Lewis sites) followed by a xylulose to furfural conversion (Brønsted sites), whereas a zeolite catalyst with primarily Brønsted sites would be more likely to catalyze a direct dehydration of xylose to furfural. It is important to note that both occur naturally in zeolites, and a thorough understanding of their respective functionalities is crucial in developing zeolites as catalysts. The nature of a zeolite's acid sites can be measured via temperature programmed desorption (TPD) experiments using various probe molecules, as discussed in Appendix B.

Acid site densities are related to the aluminum content of the zeolitic framework, where aluminum-rich species are highly acidic.[87] As more aluminum atoms are

substituted into a zeolite's framework for silicon atoms (that is, the Si/Al ratio decreases), acidity increases for two reasons. Lewis acidity increases due to incorporation and subsequent dehydroxylation of alumina, which creates coordinately unsaturated sites (CUS) capable of accepting electron pairs.[97] Brønsted acidity increases when the cation required to satisfy a newly substituted alumina tetrahedron happens to be a proton. These Brønsted acid sites consist of hydroxyl protons covalently bonded to oxygen atoms bridging silicon and aluminum atoms in the zeolite framework.[98-99]

Acid site densities are typically measured via FT-IR spectroscopy, as reported elsewhere[100-101] and as discussed in Appendix B. Also important to any discussion about zeolite acidity is the location of the acid sites; namely, sites on the molecule's external surface vs. sites within its pores. This has important implications for catalysis if there is significant acidity within the pores and the target molecules are either too large to access them (poor catalysis) or just small enough to fit in the pores and access the acid sites while excluding larger non-target molecules (potentially great catalysis).

Shape selectivity and pore dimensions are one final consideration in this discussion of zeolite catalysts. The highly specific pores and channels of a given zeolite species should be one of its primary factors for its selection for a specific catalytic goal. By matching as closely as possible the size (kinetic diameter) and shape of a reactant molecule to the pores and/or channels of its zeolite catalyst, one can vastly increase the effectiveness of the catalyst if this excludes competing non-target reactant molecules in the system. By preferentially exposing the target reactant to the acid sites within a pore or channel, the desired conversion can be achieved with high selectivity. By the same logic,

it is also important to consider the size and shape of the target product molecule in relation to the zeolite catalyst's pores and channels. If the target molecule is too large to occupy the zeolite's pore, or if it is too large to leave the pore following the reaction, this will lead to low selectivity and/or rapid deactivation of the catalyst due to full or partial blockage of the pores and their active sites. The same thought process must also be applied to any potential transition states that may occur during the reaction pathway of interest.

1.5.2 Small Pore Zeolite Catalysts

Small pore zeolites have received less attention than medium pore zeolites for converting xylose and biomass to furfural because their pore apertures (3 to 5 Å[78]) are generally too small to allow entry of xylose (6.8 Å[76-77]) or glucose (8.6 Å.[78]). Small pore zeolites have been successfully used as catalysts for the conversion of methanol to olefin,[102] but Jae et al and others[78, 103] report no formation of aromatics from glucose using several different small pore zeolites. Others cite small pore zeolites as generally unsuitable catalysts for the conversion of xylose to furfural.[104]

Despite little promise of excellent furfural production with small pore zeolites based on their pore sizes alone, others have reported a surprising amount of flexibility within the zeolitic frameworks,[105-110] allowing pore sizes to stretch by 2 Å or more. Due to their uniform networks of pores and channels, zeolites are also known for having large surface areas relative to their weight.[111] If the external surface has a sufficient density of acid sites, reactions will occur without requiring diffusion of reactants into the pores at all. In order to further analyze potential catalytic ability of small pore zeolites for biomass

upgrading, three small pore zeolites were selected to be used in this project: SAPO-34, SAPO-56, and DNL-6.

Silicoaluminophosphates, or SAPOs, are a class of molecular sieves first studied and officially classified in the 1980s. As initially reported by Lok et al of the Union Carbide Corporation, "The silicoaluminophosphates encompass a wide compositional range of O-0.3R~(Si,Al,P,)O2 in the anhydrous form, where x, y, and z represent the mole fractions of silicon, aluminum, and phosphorus and range from 0.01 to 0.98, 0.01 to 0.60, and 0.01 to 0.52, respectively, with $x + y + z = 1$."[112] They also reported that most silicoaluminophosphates show exceptional thermal and hydrothermal stabilities, and that their pore apertures range from 3 Å to 8 Å. No universal naming system is used for SAPOs, meaning that the numbers in their names do not necessarily have a systematic meaning.[113] DNL-6 is a silicoaluminophosphate molecular sieve with the RHO framework, named after Dalian National Laboratory where it was first synthesized in 2011.[114] Details about the syntheses of all three small pore zeolites are given in Appendix A.

1.6 High-Performance Liquid Chromatography

High-performance liquid chromatography (HPLC) is a powerful analytical method that uses high pressure to force solvent through a column containing fine particles that enable high-resolution separations.[115] Common components of an HPLC system, like the one used for analysis in this project, include: buffer reservoirs, a degassing unit, a pump unit, an autosampler and injector unit, a chromatography column,

and various detectors. For this project, a diode array detector (DAD) and a refractive index detector (RID) were used. Gas chromatography is often chosen over liquid chromatography because it is generally less expensive and generates less waste, but liquid chromatography is often required when the compounds of interest are not volatile enough for gas chromatography or degrade at high temperatures.[115]

HPLC chromatographic columns are expensive and are available in an enormous variety of sizes and configurations, each designed with specific separation goals in mind. In order to preserve their expensive and delicate columns from degradation, most users attempt to remove any particulate matter by passing all samples and solvents through a 0.2 μM filter prior to introducing them to the system. Users will typically also use a short guard column just before the chromatography column itself as a last attempt to remove fine particulate matter. Chromatography columns are typically packed with a solid stationary phase consisting of spherical microporous silica particles, each with a surface area on the order of several hundred square meters per gram.[115] Most HPLC buffers must be at least mildly acidic, as the silica typically becomes unstable at a pH > 8.

1.6.1 Theory behind HPLC

Two basic separation modes, normal-phase and reversed-phase, are used in HPLC along with one of two basic elution methods: gradient elution and isocratic elution. A basic knowledge of these four terms is essential to understanding the full capabilities of separation by HPLC.

In normal-phase separations, a polar stationary phase is used along with a less polar mobile phase, meaning that a more polar solvent has a higher eluent strength.[115]

Normal-phase separations work on the principle of a solute's ability to engage in polar interactions with the polar stationary phase. The more polar the solute, the more strongly it will bind to the stationary phase, leading to a longer retention times. More nonpolar solutes will bind weakly to the stationary phase or stay soluble in the relatively nonpolar buffer, leading to shorter retention times. Normal-phase separations are relatively unpopular today, due largely to inconsistent retention times caused by an inevitable presence of moisture in the buffer.

Replacing normal-phase HPLC in most applications today is reversed-phase HPLC, which uses a nonpolar stationary phase with an aqueous or polar mobile phase. Reversed-phase HPLC is insensitive to small amounts of moisture in the mobile phase, thereby circumventing one of the primary issues faced by normal-phase separations. By the same principles dictating retention times in normal-phase separations, more nonpolar analytes bond more strongly to the nonpolar stationary phase in reversed-phase HPLC and therefore have longer retention times. More polar solutes bind less strongly to the stationary phase or remain soluble in the mobile phase, and have shorter retention times. These basic separation principles can be manipulated further based on which elution method is chosen, gradient or isocratic.

Isocratic elution is used when a single mobile phase is capable of separating all solutes of interest. This requires that the solutes be of sufficiently unique polar character such that they can be fully resolved without altering the polarity of the solvent. Reversed-phase HPLC with isocratic elution was the separation technique used in this project.

Gradient elution is a more powerful technique that is most often used when isocratic separation is not capable of fully resolving multiple solutes. In gradient elution, two solvents of different polarity are typically used, with their ratio changing as the HPLC run continues, which effectively produces a polarity gradient throughout the run.[115] In a typical reversed-phase gradient separation, the ratio of solvent A to solvent B will be adjusted so as to gradually transition from being highly polar (causing polar solutes to elute fairly quickly) to being highly nonpolar (flushing nonpolar solutes from the stationary phase and causing them to elute). An example of this gradient elution is given by Harris[115] below in (Figure 12), showing increasing volume percentages of one solvent (acetonitrile) as a function of HPLC run time. Changing the solvent ratio in this way changes the polarity of the mobile phase as a whole, enabling more selective desorption of solutes from the stationary phase and elution from the column. Method development for this type of separation is a systematic process, but often must be optimized via trial and error.

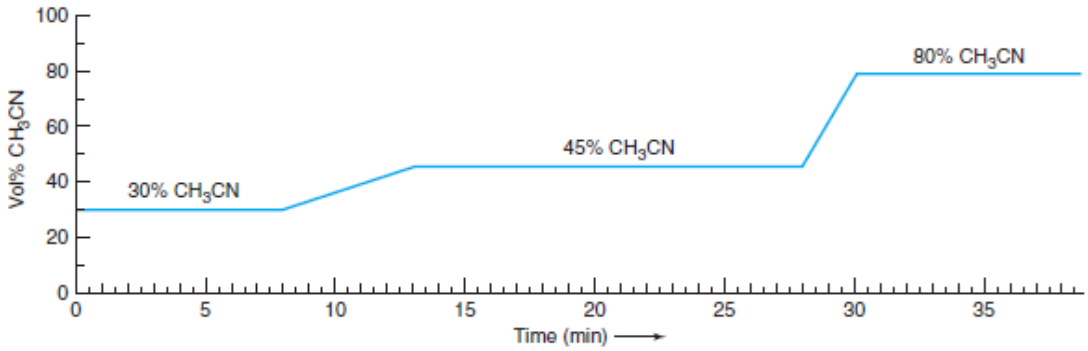

Figure 12: Example of solvent ratio changes in a typical HPLC separation with gradient elution.

Beyond these basic separation and elution modes, there are many different ways to separate components of a mixture. Harris provides an excellent decision tree designed to simplify method development (Figure 13). The precise details of each of these separation modes and the many factors governing separation are beyond the scope of this paper.

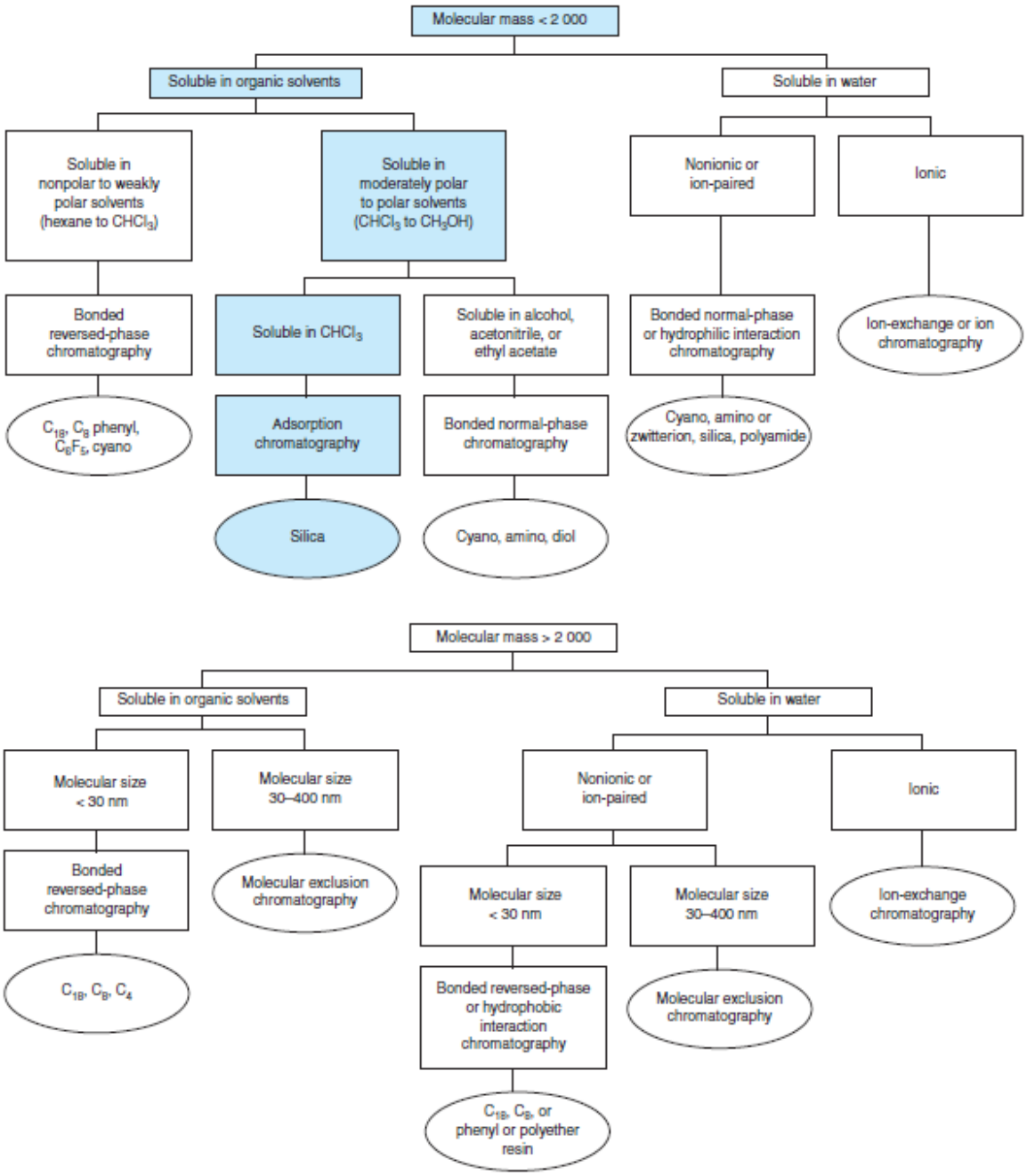

Figure 13: Decision tree for HPLC mode selection from Harris.[115]

1.6.2 Application of HPLC to this Project

For this project, two different HPLC columns were used for different aspects of the project. These are summarized below in Table 2.

Table 2: Summary of HPLC Columns Used.

Column	Part #	Manufacturer	ID (mm)	Length (mm)	Particle Size (μM)	Use
Zorbax Carbohydrate Analysis	8433000-908	Agilent Technologies	4.6	150	5	Biomass Composition Experiments
Aminex Carbohydrate Analysis	HPX-87H	Bio-Rad	7.8	300	9	Catalysis Experiments

The Zorbax column and its accompanying guard column (Agilent Technologies, 820950-908) were used in the biomass composition experiments since the HPX-87H is unable to separate xylose and glucose. The Aminex column, with its accompanying guard column (Bio-Rad, 125-0129), separates compounds based on a combination of several different mechanisms, including ion exclusion, ion exchange, and size exclusion. Ion exclusion is based on the principle that solute ions in the mobile phase will not penetrate a resin bead with a similar charge, and therefore will elute from the column more quickly than a solute ion with a dissimilar charge to the fixed charge of the resin bead. Similarly, size exclusion operates on the idea that solute molecules that are too large to penetrate the interior pores of the resin beads will travel through the column more quickly than smaller solute molecules, which physically enter the beads and elute more slowly due to a more tortuous path through the column. Ion exchange binds solute molecules to the stationary phase based on ionic interactions. Thus ions that bind more strongly to the column are retained longer than ions that only bind to the column weakly or not at all. With each of

these separation methods making up a portion of the overall separation capabilities of the Aminex column (in a proprietary way), it is able to achieve excellent separation of many different types of compounds.

1.7 Calculations

Results were quantified via HPLC, with these peak areas being calculated by the software using the manual integration functionality. Using that tool, no calculation was required to achieve peak area values for each compound of interest in any given spectra. In order to quantify these peak areas in terms of molarities, standard curves consisting of at least four data points were prepared. From these standard curves, kinetics calculations for yield, selectivity, and conversion were completed for each reaction.

1.7.1 HPLC Standard Curves

For any given compound of interest, a standard curve consisting of a minimum of four data points was generated in order to provide a means of quantifying the results of reactions. Based on estimated target molarities of each compound, standards were prepared consisting of an appropriate weight of each compound. These standards were then analyzed in triplicate via HPLC, and the average peak areas were divided by $1*10^6$ (in order to normalize the standard curves to more reasonable numbers) and plotted against the molarity of each compound in the standard. As a result, many figures in the form of Figure 14 below were generated, giving an equation for a line of best fit. Using the equation of the linear fit, the molarity of any given reaction sample could be

calculated based off of its observed peak areas. These standards were updated approximately monthly to account for any shifting of HPLC performance.

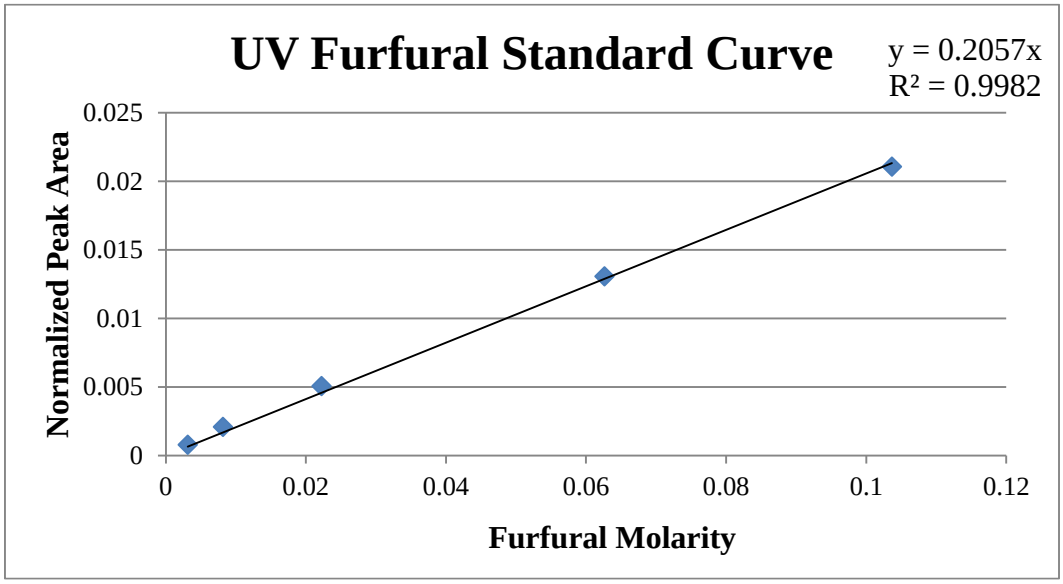

Figure 14: Example standard curve generated for analysis of furfural content following reactions.

1.7.2 Conversion Calculations

Conversion of the feed sugar is an important metric of these reactions, as it provides a quantitative measure of how far a reaction has progressed. For example, a glucose reaction that has reached a conversion of 75% tells us that 75% of the glucose that was initially present has converted to something else, whether that be target products, non-target products, or other degradation products. Monitoring conversion levels is an important way to optimize reaction conditions, primarily the lengths of reactions. Once 100% conversion is achieved, the yields of the target products are often at or near their maxima as well, and will only degrade if the reaction is continued.

To calculate conversion, one must look at the molarity of a reactant present at the start of the reaction, and the molarity of that reactant present at the end of the reaction, which is calculated from the standard curve data. For example, a reaction starting with a glucose molarity of 1.0 mol/L and ending with a glucose molarity of 0.25 mol/L would result in a conversion of 75%, and is calculated as follows:

[1 - (Final Molarity/Initial Molarity)]*100% = % Conversion

[1-(0.25 M/1.0 M)]*100% = 75% Conversion

1.7.3 Selectivity Calculations

Selectivity is a metric used to quantify how much of the target product is being produced in relation to other non-target products. It is calculated by taking the final moles of the target product, and dividing that number by the total number of moles of reactant that actually reacted (in other words, starting moles of reactant minus final moles of reactant).

[(Final Moles Furfural)/(Initial Moles Gluc – Final Moles Gluc)]*100% = % Selectivity

[(0.45 Moles Furfural)/(1 Mole Gluc – 0.25 Moles Gluc)]*100% = 60% Selectivity

Selectivity is a way to gauge how effective a given catalyst is for the desired reaction. Decent yields can still be achieved with low selectivities, but by knowing an exact value for selectivity, the researcher can pinpoint exactly how well his/her catalyst is aiding the desired reaction.

1.7.4 Yield Calculations

As discussed above, final molarities of each compound of interest were calculated based on peak areas in the HPLC spectra. Yield is calculated by multiplying the calculated values of conversion and selectivity as follows:

(% Conversion) * (% Selectivity) = % Yield

(75% Conversion) * (60% Selectivity) = 45% Yield

Calculating yield in this manner enables a comparison across multiple types of reactions and initial conditions, versus using absolute yield values. In this way, one can still directly compare percent yield values for a reaction starting with different reactant loading amounts.

2.0 MATERIALS AND METHODS

In this study, several types of zeolite and metal-organic framework (MOF) molecules were evaluated for use in the conversion of xylose and switchgrass to furfural. The catalyst reacted in glass vials with xylose and switchgrass in a solvent system consisting of 90/10 γ-valerolactone (GVL)/water. Studies to characterize the recyclability of these zeolites and whether or not acid sites leach into solution were also carried out. All results were quantified via HPLC and GC/MS, among other techniques.

2.1 Catalyst Synthesis

All zeolites and MOFs were synthesized by a collaborating research group led by Dr. Moises A. Carreon at the Colorado School of Mines (CSM) in Golden, CO. The SAPO-34 that was obtained commercially (ACS Material, LLC) is referred to henceforth as SAPO-34C. Zeolite Rho,[116] ZIF-8,[117] ZIF-67,[117] Cu-MOF,[117] SAPO-34,[118] SAPO-56,[119] and DNL-6[116] were all synthesized according to previous literature. Specific details of the syntheses carried out by Dr. Carreon's group are provided in Appendix A.

2.2 Catalyst Preparation

In order to remove any residual water or contaminants and achieve an accurate weight measurement, all zeolites were baked overnight prior to use at 573 K (Thermo Scientific Thermolyne Furnace Model F47925-80 and Fisher Scientific Isotemp Muffle Furnace Model 182). The 0.02 M sulfuric acid (SA) and Amberlyst-70 (A70; Dow Chemical) catalysts provided benchmarks to previously published studies. The 0.02 M

SA was prepared from 18 M SA (Fisher Scientific, A300-212) and stored at 275 K (Fisher Scientific refrigerator). A stock solution of 0.2 M SA was first made by adding 2.00 mg (0.2 mol) of pure sulfuric acid to 1 L of water. This stock solution was then diluted 10x when preparing reaction vials, to achieve a concentration of 0.02 M for all reactions using SA as catalyst. The A70 was crushed into a fine powder using a mortar and pestle and rinsed with water until the wash water had a pH of ~7 (Fisher Scientific Accumet AB15 pH meter). The crushed and washed A70 was baked at 378 K overnight prior to use (Thermo Scientific Thermolyne Furnace, Model F47925-80).

2.3 Catalyst Characterization

The small pore zeolites were characterized at the Colorado School of Mines and Syracuse University by collaborators using x-ray diffraction (XRD), scanning electron microscopy (SEM), Brunauer-Emmet-Teller (BET) theory surface area analysis, and temperature programmed desorption.

All materials were characterized by physisorption of N_2 at 77 K (Micromeritics ASAP 2020). Prior to N_2 dosing, samples were evacuated at 363 K and subsequently outgassed under vacuum (623 K, 4 h). This enabled calculations of surface area for each small pore zeolite via BET theory, which was carried out by a collaborating research group led by Dr. Jesse Q. Bond at Syracuse University. Brønsted and total acid site densities were also determined by Dr. Bond's group; their procedures are given in greater detail in Appendix B.

2.4 Xylose and Switchgrass Conversion Reactions

Experiments were carried out in 10 mL glass reactors (Kimble-Chase, 60702-10) sealed with a Teflon septum (Kimble-Chase, 73818-24) and polypropylene cap (Kimble-Chase, 75201G-24400) at 448 K or 463 K in a heated oil bath (Fisher Scientific, 5159-500) with magnetic stirring (Fisher Scientific Isotemp) (Figure 15). Temperature of the oil bath was monitored with two additional reference probes to verify consistent bath temperature.

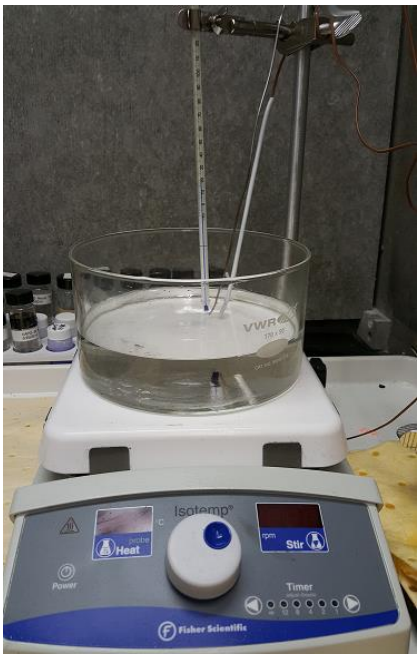

Figure 15: Oil bath setup with magnetic stirring and three independent temperature probes.

Dehydration of xylose (Sigma-Aldrich, X1500-500) to furfural was carried out in 4.0 g of 90 wt% γ-valerolactone (GVL; Acros Organics, 140795000)/10 wt% water (18.2 milliQ) solvent with 2 wt% (0.082 g) xylose or switchgrass (obtained through Brett Allen at the Sidney, MT USDA) added to the reactor. Then, catalyst was added in the amount

of 0.02 M sulfuric acid or 0.048 g of solid acid catalyst. The reactors contained triangular stir bars (Fisherbrand, 1451371), were placed in a heated oil bath, and stirred at 600 rpm for the reaction time.

Likewise, 2 wt% glucose (Fisher Scientific, D16-500) and 2 wt% switchgrass reactions were prepared in the same way. These vials were sealed as previously mentioned and placed back into the 463 K oil bath and stirred for the stated reaction time. All results were analyzed via HPLC (Agilent 1100, BioRad Aminex HPX-87H column, RI and DA detectors; see section 2.8) and quantified via analysis of standards consisting of various concentrations of xylose and furfural (Sigma-Aldrich, 185914-100) in 90/10 GVL/water.

2.5 Catalyst Leaching Studies

In glass vial reactors, 0.048 g of catalyst in a 90/10 GVL/H_2O solvent system (consists of approximately 4.50 g of GVL and 0.50 g of H_2O) was added to the vial and sealed with a septum and polypropylene cap and then placed in a 463 K oil bath and stirred for a set amount of time based on the time required to achieve approximately 50% conversion in xylose conversion reactions (Section 2.8; 1 h for blank and SAPO-34C and for 0.25 h A70) on a hot/stir plate. The catalyst was separated from the solvent by centrifugation (Thermo Scientific Sorvall ST 8) at 8000 rpm for 10 minutes (Figure 16), and 4.00 g of the solvent was decanted into a new vial containing approximately 0.082 g of xylose to make a 2 wt% xylose solution. Then the reaction was run as stated in section 2.4.

Figure 16: Centrifuge used to separate solid catalyst from solvent following reaction.

2.6 Catalyst Recyclability Studies

Recyclability studies were carried out as a proof of concept with SAPO-34C to determine the reusability of these small pore zeolites. Three rounds of reactions were run with both SAPO-34C (1 h at 463 K) and with A70 (5 min at 463 K). These reaction lengths were chosen as past experiments with both catalysts have produced moderate conversions at these respective time points. A first round of reactions consisted of six reaction vials for both catalysts, each consisting of 0.048g catalyst and 2 wt% xylose in a 90/10 GVL/water solvent system. Following the reactions, the catalyst was separated via centrifuge as described in section 2.5, recovered from each vial, combined, and washed

with 5 x 25 mL portions of acetone. SAPO-34C was then baked overnight at 573 K and A70 at 378 K. A second round of reactions consisted of four reaction vials for each catalyst, with reactions occurring under the same conditions as before. Once again, the catalysts was recovered, combined, washed, and baked prior to running a third round of reactions, this time with two reaction vials for each catalyst. Data was analyzed via HPLC (Agilent 1100, BioRad Aminex HPX-87H column, RI and DA detectors; see section 2.8) for each individual reaction vial.

2.7 Biomass Composition Analysis

Switchgrass was obtained through Brett Allen from the Northern Plains Agricultural Research Laboratory in Sidney, MT. Biomass composition analysis was completed following the National Renewable Energy Laboratory's Laboratory Analytical Procedure (NREL LAP) TP-510-42618. Using a water bath, the switchgrass was hydrolyzed in a 120 mL pressure tube (Ace Glass, 8648-30) with plug (Ace Glass, 5845-47) with 72% sulfuric acid prepared from 18 M sulfuric acid (Fisher Scientific, A300-212) at 303 K in an oil bath for 1 h while stirring every 10 min using a triangular Teflon coated stir bar on a combination stirring and heating plate. After 1 h, the solution was diluted with deionized water to an acid concentration of 4% and placed in an autoclave (Market Forge Industries, STM-E; located in the Center for Biofilms EPS325) for 1 h at 394 K. Liquid samples were neutralized to a pH of approximately 6 and filtered using 0.2 μm filters (Agilent, 5190-5265) for HPLC analysis. Results were quantified using an Agilent Zorbax Carbohydrate column (Agilent 1100; 75:25 (by volume)

acetonitrile:water mobile phase) with a refractive index detector for xylose and glucose (see section 2.8) analysis. These data were compared to sugar recovery standards made as stated in the NREL LAP.

2.8 Analysis

2.8.1 High Performance Liquid Chromatography

All results were analyzed via HPLC (Agilent 1100, BioRad Aminex HPX-87H column, RI and DA detectors, Figure 17 below) and quantified via analysis of standards consisting of various concentrations of xylose (retention time of 9.8 min with RID), glucose (retention time of 9.2 minutes with RID), furfural (retention time of 52 min with DAD at a wavelength of 286 nm), HMF (retention time of 33 minutes with DAD at a wavelength of 286 nm) in 90/10 GVL/water. A GVL peak is not detectable via DAD with the wavelength set to 286 nm. Two different columns were used: an Agilent Zorbax column (part number 843300-908) for xylose and glucose analysis in the biomass composition experiments and a BioRad Aminex HPX-87H column for xylose, glucose, HMF, and furfural analysis of all xylose, glucose, and switchgrass conversion experiments.

Figure 17: HPLC with RID and DAD used for analysis of all experiments.

The Zorbax column used a mobile phase buffer solution consisting of 75/25 acetonitrile (Fisher Scientific, A955-4)/water by volume. The Aminex column used both 5 mM sulfuric acid for early experiments and 10 mM trifluoroacetic acid (TFA, Acros Organics, 13972-5000) for later experiments as mobile phase buffer. All buffers were passed through 0.2 μm filters prior to use (Figure 18).

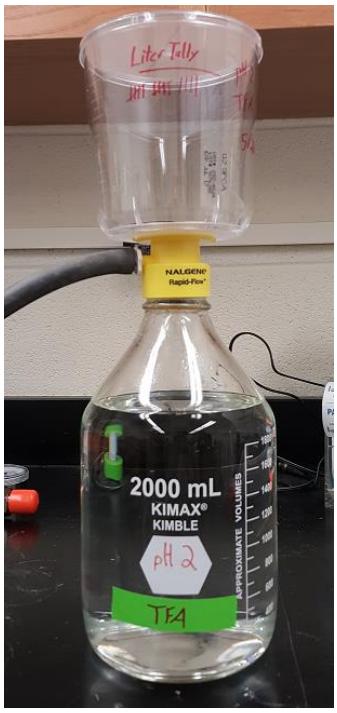

Figure 18: All HPLC buffers were passed through a 0.2 µM vacuum filtration system.

The 5 mM sulfuric acid (pH ~2) was made with 10 mL 0.5 M sulfuric acid (Acros Organics, AC124240025) made up to 1 L with 18.2 milliQ H_2O (Barnstead Smart2Pure 3). The solvent flow rate was 0.6 mL/min, and the system pressure and temperature were 72 bar and 323 K, respectively. For the later experiments, the 10 mM TFA solvent was used and made with 1.50 mL of TFA in 2 L (total) of 18.2 milliQ water.

Both columns utilized the same HPLC settings, which consisted of the following: 0.6 mL/min flow rate of solvent, 323 K RID temperature, 323 K column compartment temperature, and an approximately 1 h run time due the produce retention times (Table 3). Data was analyzed and peaks were integrated manually via Chemstation software. An overview of the Chemstation (Rev A.10.02) is shown below in Figure 19.

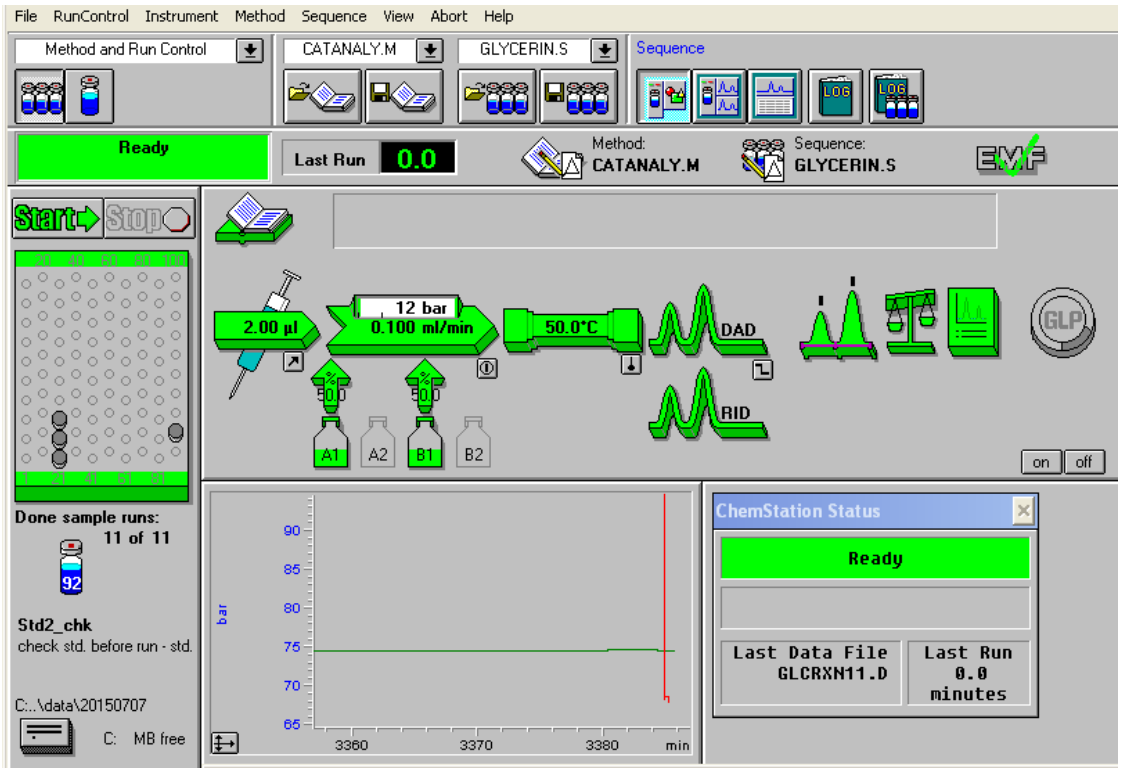

Figure 19: Overview of Chemstation run control software. Injection volume, flow rate, column temperature, and DAD & RID settings are controlled from here.

Table 3: Approximate HPLC retention times of chemicals analyzed.

Chemical	**Column**	**Detector**	**Approx. retention time (min)**
Xylose	Zorbax	RID	7.9
	Aminex	RID	9.8
Glucose	Zorbax	RID	8.5
	Aminex	RID	9.2
GVL	Aminex	DAD (286 nm)	Not Detectable at this Wavelength
Furfural	Aminex	DAD (286 nm)	52
HMF	Aminex	DAD (286 nm)	33
Levulinic Acid	Aminex	RID	17

All samples and standards were passed through 0.2 µm filters (Agilent, 5190-5265) attached to Luer-Lok style syringes (BD, 309657) prior to being injected, as seen in Figure 20 below.

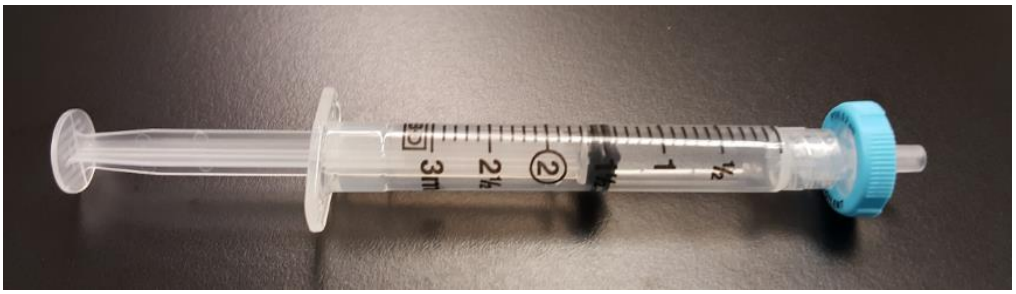

Figure 20: Syringes with 0.2 μM filters were used to filter all samples and standards.

When not in active use, the HPLC was set to a standby mode that consisted of the following: 0.1 mL/min flow rate, 323 K RID temperature, 323 K column compartment temperature, and the UV bulb turned off. This was done in order to minimize unnecessary resource use. All acidic effluent waste was neutralized to a pH of 7 and flushed down the sink with at least 10:1 water:waste. Organic effluent waste was saved in 4 L amber glass jars to be picked up by MSU's Safety & Risk Management department for proper disopsal.

Significant maintenance was required by the HPLC throughout the course of this project; more details of the issues, troubleshooting, and maintenance that took place are given in Appendix C.

2.8.2 Karl Fischer Titration

In order to determine the water content of the solvent, a Karl Fischer Titration system was used (Denver Instruments Model 275KF titration module connected to a Denver Instruments Model 260 titration controller, Figure 21 below).

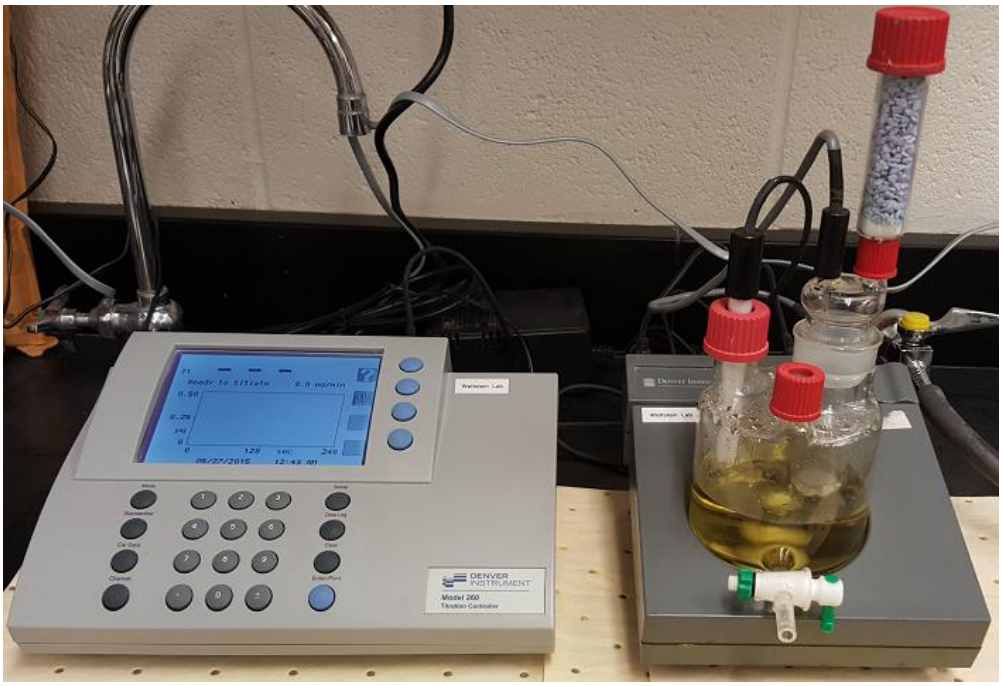

Figure 21: Karl Fisher titration instrumentation.

HYDRANAL-Coulomat AG (Fluka Analytical, 34836-500) was used as the anolyte reagent and HYDRANAL-Coulomat CG (Fluka Analytical, 34840-50) was used as the catholyte. 5 mL of catholyte was added to the small cathodic compartment and anolyte was added to the large anodic compartment to the same level as the catholyte (approx. 100 mL). Three replicate injections of 2 g of solvent were made through a septum into the titration cell using a 3 mL syringe with a luer lok needle. Three replicate injections of 1.5 g of a 1 wt% water standard (Fluka Analytical, 34849-80) were made to verify instrument performance. The weight of the syringe when full and when empty are input into the titration controller, and a solvent injection amount in grams is calculated automatically. The system then automatically performs a titration and calculates the water content of the solvent, displayed in wt% water. Anywhere between 1 g and 3 g of solvent are sufficient injection amounts, and make no difference in the result

3.0 RESULTS

The potential for the catalytic conversion of xylose, glucose, and switchgrass to furfural was studied in detail with several small-pore zeolites and MOFs using pure xylose, glucose, and switchgrass in 90/10 wt% GVL/water solvent systems. More specific details about the SAPOs used in this study are given below in Table 4, where "SAPO-34C" denotes commercially purchased SAPO-34 and "SAPO-34" and "SAPO-56" denote catalysts synthesized by Dr. Moises A. Carreon's collaborating research group at the Colorado School of Mines in Golden, Colorado, USA.

Table 4: Chemical and structural properties of the small pore zeolites and ZSM-5, as determined experimentally (acid site and surface area data) and as found in the literature (pore size).

	Total acid sites ($\mu mol/g_{cat}$)	Brønsted acid sites ($\mu mol/g_{cat}$)	Surface area (m^2/g)	Pore size (Å)	Framework Type
SAPO-34C	980	1100	510	3.8[78]	CHA[120]
SAPO-34	370	400	520	3.8[78]	CHA[120]
SAPO-56	590	240	360	3.6[121]	AFX[122]
DNL-6	270	220	140	3.6[123]	RHO[124]
ZSM-5	---	31	425	5.5[81]	MFI[125]

3.1 Catalysts

3.1.1 MOFs

All of the MOFs and zeolite Rho studied resulted in less than 2% furfural yield from xylose. Due to the higher yields from small pore zeolites, the zeolites became the focus of this study.

3.1.2 Small Pore Zeolites

Of the four small pore zeolites used in this study, three were synthesized: SAPO-34, SAPO-56 and DNL-6. These had XRD patterns consistent with CHA, AFX, and RHO, respectively (Appendix B). Both the XRD patterns (Figure 28) and SEM images (Figure 29) of the synthesized zeolite crystals are shown in Appendix B. SAPO-34 and SAPO-56 showed cubic-like morphology with average sizes in the 1-5 μm range and 0.5 μm, respectively. DNL-6 has a hexagonal-like morphology with an average size of 4 μm. One commercial catalyst was also obtained: SAPO-34 (ACS Materials; referred to as SAPO-34C). For all reactions, 0.048 g of catalyst and a solvent blend of 90/10 wt% GVL/water was used unless otherwise noted.

3.2 Reactions

In order to probe the capabilities of these small pore zeolites as catalysts for the deconstruction of switchgrass and the dehydration of glucose and xylose to furfural, many individual reactions were executed, ranging in length from 5 minutes to 24 hours. A preliminary reaction temperature study was carried out prior to the other experiments. By increasing the reaction temperature from 448 K to 463 K, higher furfural yields were achieved in shorter amounts of time. These results using SAPO-34C are summarized in Figure 22.

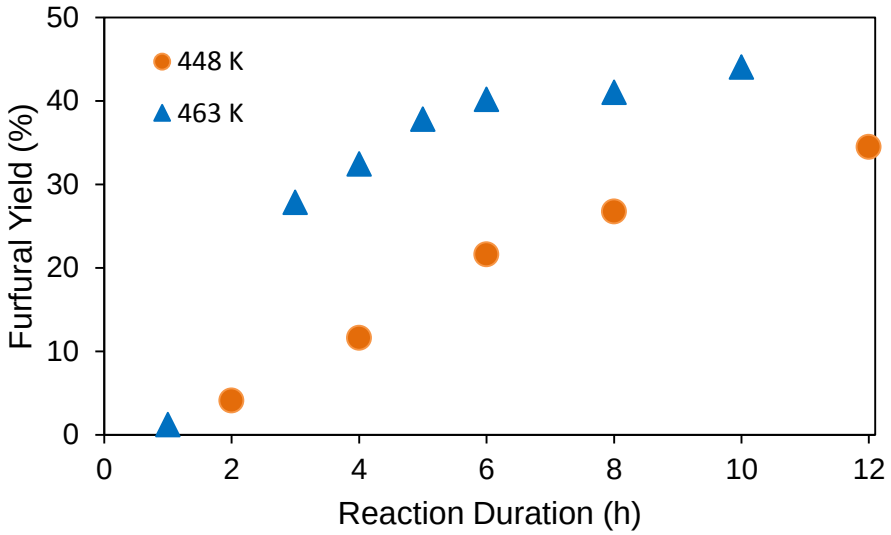

Figure 22: Results of reaction temperature study with SAPO-34C, showing furfural yields at 448 K (circles) and 463 K (triangles).

3.2.1 Reactions with Xylose

After 0.25 h, both the 0.02 M sulfuric acid (SA) and Amberlyst-70 (A70) had high furfural yields (63% and 67%, respectively; Figure 23), which is similar to previous results.[19] Analogously, the ZSM-5 produced a furfural yield of 70% after a 6 h reaction, which is also similar to previous results.[19] The SAPO catalysts produced moderate furfural yields, in the range of 30% to 40%. While these yields are lower than those achieved with A70 and SA, they are substantially higher than that which was achieved in a blank reaction containing no catalyst. With the DNL-6 catalyst, furfural yields were no higher than achieved in the blank reaction, indicating that DNL-6 does not provide any notable benefit over no catalyst in reactions starting from pure xylose. Representative error bars are included on just one data point in Figure 23 and in all subsequent figures. In these reactions, the major source of error is derived from fluctuations in the

temperature of the oil bath (thereby affecting the reaction temperature). Each time a vial is added to or removed from the bath, slight temperature fluctuations occur, which are then typically exacerbated as the system overcorrects before settling back to the desired temperature.

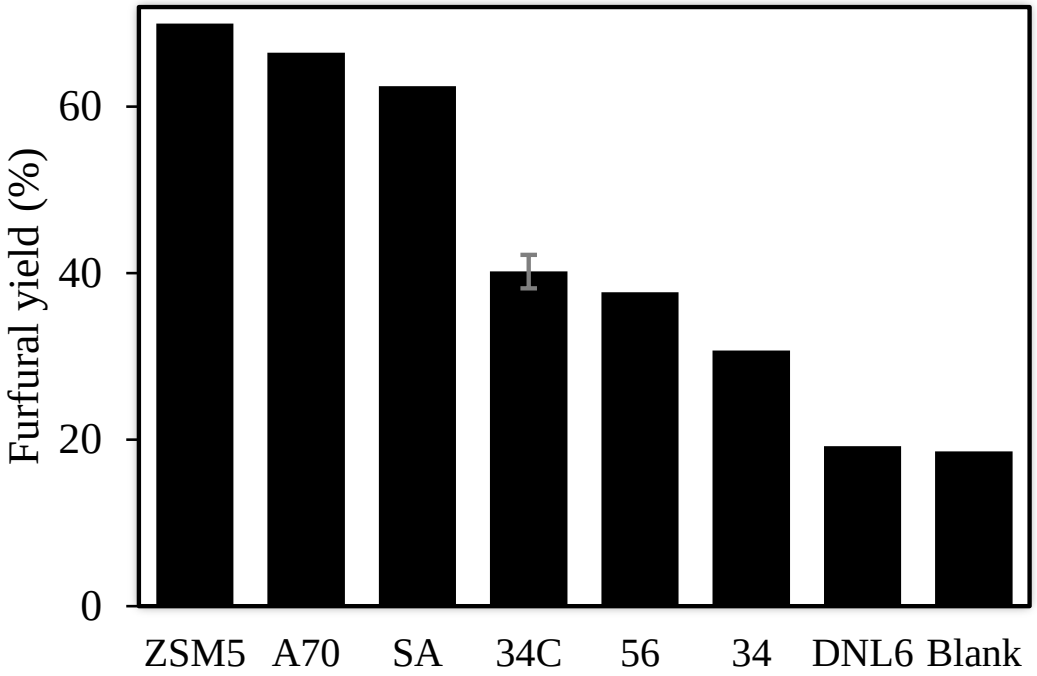

Figure 23: Furfural yields from 2 wt% xylose in 90/10 GVL/water at 463 K for 0.25 h for A70 (Amberlyst-70) & 0.02 M sulfuric acid (SA) and 6 h for all others. Blank = no catalyst; 56, 34C, and 34 = SAPO-XX.

3.2.2 Reactions with Glucose

Other researchers[19, 126-127] have shown that furfural can be produced from glucose via the following mechanism: glucose reacts to form formaldehyde and furfural[126] by the keto-enol tautomerization of glucose, followed by the formation of a pentose through a retro-aldol reaction, which finally undergoes dehydration to form furfural.[127] The conversion of glucose in 90/10 GVL/H_2O resulted in maximum furfural yields of 25%

(0.5 h), 14% (0.25 h), and 9% (11 h) from SA, A70, and SAPO-34C, respectively, along with production of levulinic acid and 5-hydroxymethylfurfural (HMF). Blank reactions with glucose in 90/10 GVL/H_2O showed furfural yields of up to 7%, but only after exceedingly long reaction times (24 h and longer). Formaldehyde was detected in low amounts (less than 5% yield) in the reactions, and although formaldehyde is formed in a 1:1 molar ratio with furfural, acidic conditions and high temperature cause degradation and side reactions leading to decreased formaldehyde concentration.[128] Despite this lack of a 1:1 ratio of furfural:formaldehyde, the presence of formaldehyde at all does lend support to the reaction mechanism of glucose to furfural mentioned above.

3.2.3 Reactions with Switchgrass

For the switchgrass experiments, 1 and 2 wt% switchgrass feeds both resulted in almost complete biomass solubilization and yields of furfural were greater than with higher loading weights of switchgrass (Figure 24). Because there appeared to be diminishing returns when starting with a switchgrass amount greater than 2 wt%, a loading of 2 wt% was chosen to be used for all switchgrass reactions. At the higher amounts of switchgrass, complete solubilization of the biomass was challenging. When solids remained in the vial following a reaction, separation and reclamation of the used catalyst were much more difficult than in reactions with complete solubilization of the biomass. With a primary goal of these studies being to develop solid catalysts that are easily recycled, easy separation of spent catalyst is a critically important attribute.

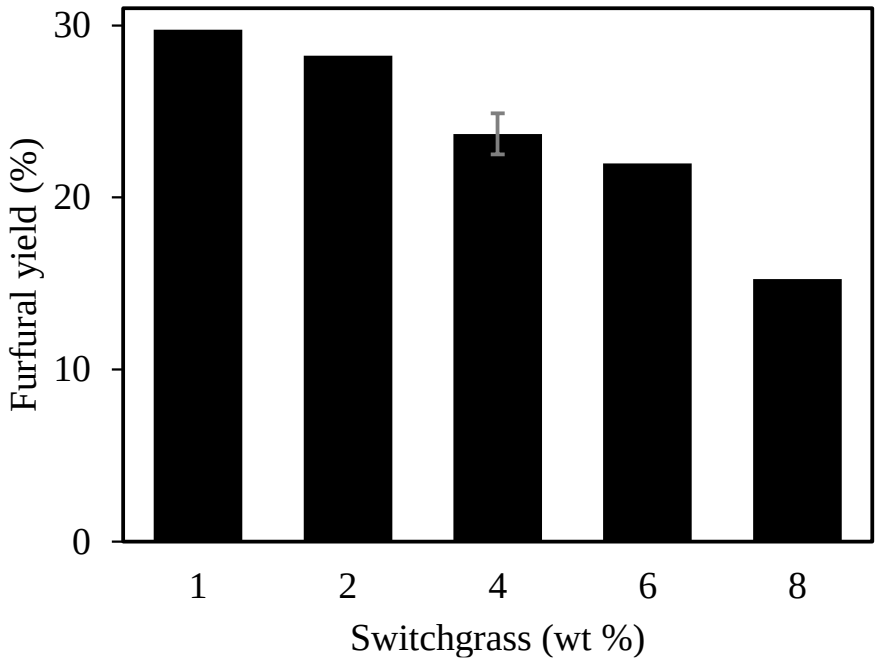

Figure 24: Furfural yields after 8 h of reaction with SAPO-34 at 463 K are compared for various starting amounts of switchgrass in 90/10 GVL/water.

Since the switchgrass contains both xylose (18 wt%) and glucose (31 wt%), furfural yields for the switchgrass reactions were calculated based on the reaction mechanisms that each mole of xylose and of glucose initially present can convert to furfural in a 1:1 ratio. Therefore, the molar yield of furfural from the experiment divided by the initial molar quantity of xylose and glucose equaled the calculated furfural yield. Just as with xylose and glucose as the starting material, reactions were performed using 2 wt% switchgrass with the small pore zeolites, SA, and A70 (Figure 25).

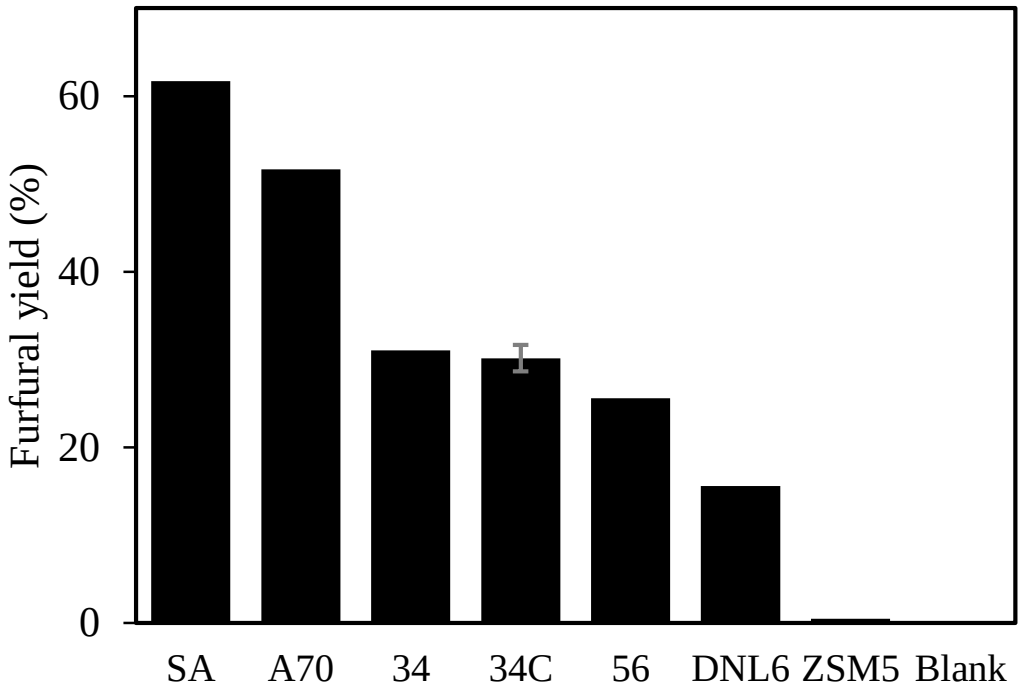

Figure 25: Furfural yields (actual furfural moles / (initial xylose + glucose moles)) from 2 wt% switchgrass in 90/10 GVL/water at 463 K after 0.5 h for A70 (Amberlyst-70) & 0.02 M sulfuric acid (SA) and 24 h for all others. Blank = no catalyst; 56, 34C, and 34 = SAPO-XX.

Once again, note that the SA and A70 achieved high yields of furfural after a relatively short reaction time. Similar to the xylose reactions, the SAPOs again achieved moderate yields of furfural in the 30% range. Most importantly, the blank reactions (no catalyst) starting from 2 wt% switchgrass achieved zero furfural yield. Thus, in this case, even though the DNL-6 achieved a fairly low furfural yield, it is still markedly higher than that achieved by the blank. This indicates that an acid catalyst is essential for the deconstruction and conversion of biomass, whereas previously, the blank reaction was capable of converting pure sugars.

3.2.4 Blank Reactions and Solvent Effects

Mellmer et al. showed that using GVL as a solvent for xylose dehydration changes the activation energy of the reaction, resulting in increased reaction rates and enhanced product selectivity.[129] Although the 90/10 GVL/water solvent system catalyzed the xylose dehydration reaction without additional catalyst present, the reaction time required to reach the maximum furfural yields was shorter with the zeolite catalysts. With no catalyst, 24 h was required to reach a maximum furfural yield of 30%, while SAPO-34C, SAPO-56, and SAPO-34 all surpassed 30% yield within 4 h. Blank reactions with and without catalyst (SA) but with no sugars in 90/10 GVL/water showed zero furfural yield, which confirmed that GVL was not converting into furfural or had furfural initially present. This was considered because GVL is itself also derived from biomass and has a similar chemical structure to furfural, so there is possibility of contamination of the GVL with furfural or even conversion of GVL to furfural.

3.2.5 Leaching and Water Dissociation

Because of the moderate yields achieved in the blank reactions, water dissociation was considered since it becomes increasingly favorable at high temperatures where the intermediate protons could potentially catalyze xylose dehydration.[130-131] To test this, xylose dehydration was carried out with no catalyst for 24 h in pure GVL, which contained 0.11 wt% water (as determined by Karl Fischer Titration), and a 28% furfural yield was achieved. To verify the performance of the Karl Fischer Titrator, three replicate injections of a 1 wt% water solution were also made, with an average water content calculated to be 0.94 wt% ± 0.02 wt%. An analogous reaction was performed, using

90/10 GVL/water as the solvent, and a nearly equivalent furfural yield of 30% was achieved. This supports the hypothesis that the zeolites, rather than water dissociation, provide the acidity necessary to catalyze xylose dehydration within shorter reaction times.

Gurbuz et al. found that the A70 acts as a homogeneous catalyst in GVL/water systems,[19] which was confirmed in this project with a leaching study using A70 that resulted in a furfural yield of 57% when a solvent previously exposed to A70 was used (Figure 26).

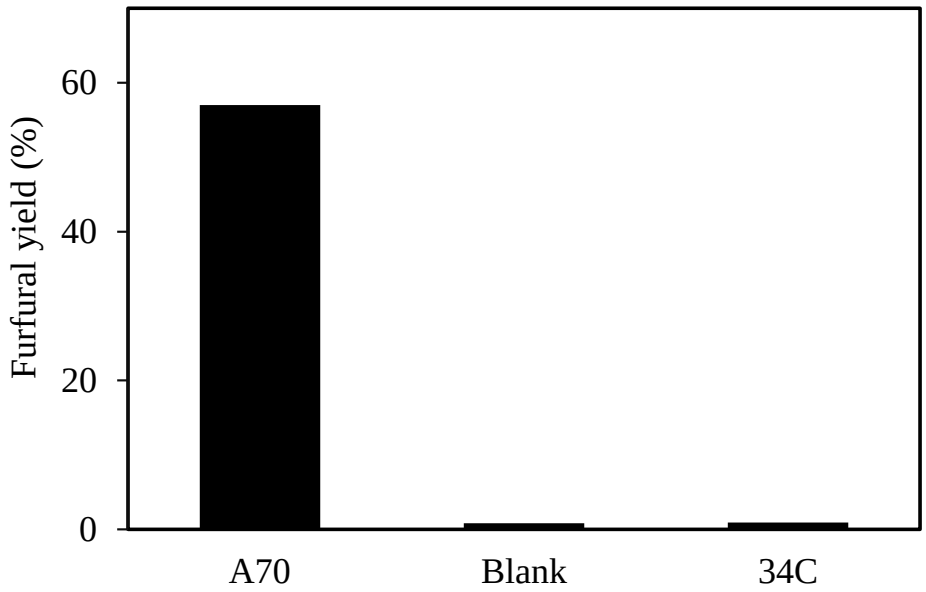

Figure 26: Furfural yields from leaching reactions with A70, blank (no catalyst), and SAPO-34C in 90/10 GVL/water.

A significant amount of acid sites leached from the A70, allowing the reaction to likely be catalyzed homogeneously. Carrying out the same leaching study procedure for SAPO-34C resulted in low furfural yields that were equivalent to a blank solvent (Figure 26), which confirms that the reaction occurred heterogeneously on the zeolite catalysts. This

has implications in the reusability of these catalysts, with the non-leaching SAPO-34C likely able to be reused multiple times while the A70 loses activity due to loss of acid sites over multiple rounds of reaction.

3.3 Recyclability Studies

Catalyst recyclability experiments showed that SAPO-34C can be recycled and still maintain high catalytic effectiveness. The furfural yield only decreased 5% from the first reaction to the second, and then the yield held constant for the third reaction (Figure 27).

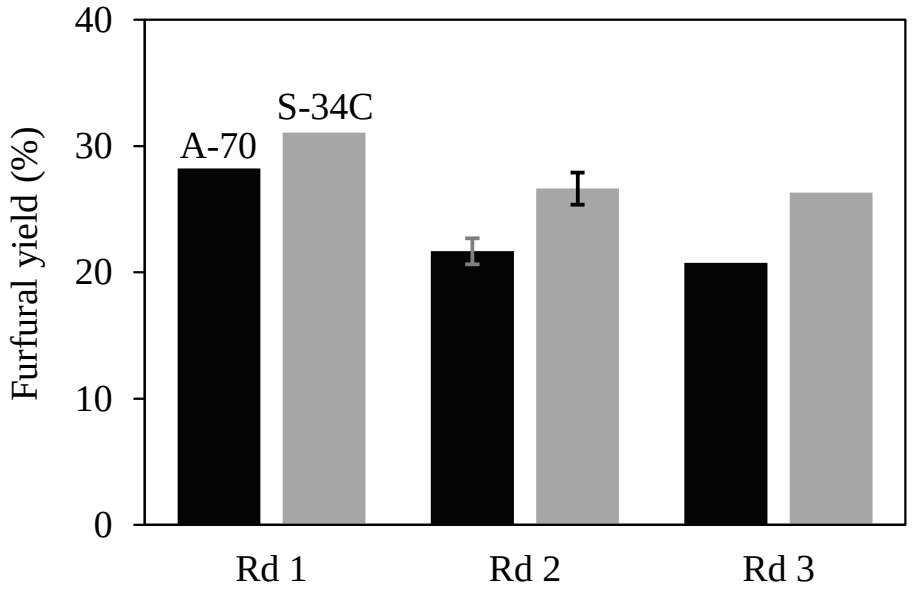

Figure 27: Recyclability experiment results showing furfural yields A70 (black) and S-34C (gray) through three sets of experiments (i.e. “RD 1”, “RD 2”, and “RD 3”).

The decrease in furfural yield from the first to the second reaction may be related to the surface deposition of carbonaceous species leading to the blockage of some active sites, causing a slight decrease in catalyst activity. This behavior has been previously

observed and reported for SAPO-34 by Suprun et. al.[132] They hypothesized that the relatively high acidity and small pores of SAPO-34 are both factors that lead to accumulation of carbonaceous deposits blocking its surface, which could be partially avoided with a lower reaction temperature.[132] Between each round of reaction, the spent catalyst was washed and then baked at 573 K, which may be sufficient to remove most carbonaceous deposits in or on the catalyst.

3.4 Potential Reaction Mechanism Discussion

Although the zeolites contain a significant number of internal acid sites, the pore sizes of the zeolites (3.6 - 3.8 Å) should hinder xylose diffusion because of the size of the molecule (~6.8 Å[76-77]). Reactions performed with the SAPO-34 and SAPO-56 templates in place (that is, prior to calcination) resulted in furfural yields equivalent to those obtained in blank reactions under the same conditions. (For these reactions, 0.050 g of catalyst was used instead of 0.048 g because the weight of the template was about 4 wt%.) This may indicate that the reaction does not take place on the surface of the zeolite, but that the sugar molecules are somehow gaining access to the interior acid sites. Many groups have reported that zeolites have flexible frameworks,[105-110] and thus the reaction conditions used may have allowed the SAPO framework to flex, thereby dynamically exposing the internal acid sites to xylose and/or glucose. To measure this more definitively, in-situ pore size measurements would have to be made while accounting for the temperature, pressure, and other conditions observed during a typical reaction. The total acid site concentrations, determined experimentally via ammonia and ethylamine

temperature-programmed desorption in combination with surface area, do correlate with observed furfural yields, indicating that Brønsted acid sites are a critical component for the reaction, which is frequently confirmed in the literature.[20, 50, 79, 85, 133]

4.0 CONCLUSIONS

Moderate furfural yields were achieved from both xylose and switchgrass with small pore zeolites SAPO-34 and SAPO-56 in 90/10 GVL/water. These catalyzed reactions produced substantially higher yields than blank reactions containing no catalyst starting from xylose, glucose, and switchgrass.

While higher furfural yields were achieved with SA and A70, there is strong potential for small pore zeolites as catalysts for biomass upgrading. The results of the leaching experiments performed in this study indicated significant acid site leaching and therefore, homogeneous catalysis with A70. On the other hand, SAPO-34C showed insignificant leaching and likely, heterogeneous catalysis. Unlike with A70, SA, and other homogeneous catalysts, these small pore zeolites are easy to separate and reuse following a reaction. More generally, heterogeneous catalysis is advantageous over homogenous catalysis because solids are typically much easier to separate and reuse. Using heterogeneous catalysts also eliminates the need for neutralization of mineral acids before disposing of them as waste. In addition to being easily separable following a reaction, the SAPO-34C catalyst recycles multiple times with only a slight drop in furfural yield.

Although blank reactions (containing no catalyst) were able to achieve low-to-moderate furfural yields when starting from pure xylose or glucose, zero furfural yield was attained in blank reactions from switchgrass. This indicates that an acid catalyst is critical to deconstruct actual biomass and upgrade it to platform chemicals like furfural.

Other classes of molecules, such as medium pore zeolites, have garnered significantly more attention in the upgrading of biomass to furfural. At the time of completion of this study, this is the first known demonstration of any furfural yields from biomass with small pore zeolites. Although others have achieved higher furfural yields with medium pore zeolites, small pore zeolites could still see critical use in situations requiring higher hydrothermal stability than is achievable with most medium pore zeolites. ZSM-5, one of the most ubiquitous medium pore zeolites in use today, shows fairly substantial deactivation at high temperatures in the presence of steam.[134-135] Conversely, small pore zeolites often show high hydrothermal stability,[136-137] with SAPO-34 in particular exhibiting exceptional hydrothermal stability.[138] This enhanced stability could enable small pore zeolites to be used under more extreme reaction conditions where medium pore zeolites and other common catalysts may show considerable degradation.

Additionally, these small pore zeolites may be synthesized under conditions that allow their structures to be optimize the strength, location, and nature of their acid sites for the upgrading of biomass to furfural.[139-141] Hypothetically, a reaction could be designed to take advantage of the surface acidity of a small pore zeolite for the dehydration of sugar molecules to furan compounds. A reaction within the pores by the smaller furan compounds to further upgrade them to even more useful platform chemicals would facilitate using a single catalyst. This “tuneability”, coupled with excellent hydrothermal stability, should keep small pore zeolites firmly implanted in the continuous innovation of biomass upgrading technologies.

These results also raise several questions to be addressed in future studies as to the mechanism by which these catalysts actually convert xylose and glucose to furfural. Based on their small pore sizes and relatively low surface acidity, one would not necessarily expect significant furfural production with these small pore zeolites, if any at all. Medium pore zeolites are typically thought to be better suited to biomass upgrading due to pore apertures that are closer in size to the component sugar molecules of biomass. Despite these challenges, moderate furfural yields were repeatedly achieved with the small pore SAPO zeolites used in this study. Further studies will be required at the fundamental level to analyze exactly where on these zeolites the conversions of interest are taking place. With that knowledge, there could be a major increase in use of these small pore zeolites for biomass upgrading in innovative ways.

APPENDICES

APPENDIX A

SYNTHESIS OF CATALYSTS

All catalysts used in these studies were synthesized by a collaborating research group led by Dr. Moises A. Carreon at the Colorado School of Mines in Golden, CO. As SAPO-34, SAPO-56, and DNL-6 showed vastly more potential in this application than zeolite Rho and the various MOFs also analyzed in these experiments, their precise synthesis details are given below.

SAPO-34

SAPO-34 was synthesized employing a procedure reported elsewhere.[118] In a typical synthesis, the Al source (99.9% $Al(i\text{-}C_3H_7O)_3$), H_3PO_4 and deionized water were stirred for 3 h to form a homogenous solution. Then, Ludox AS-40 colloidal silica (40 wt% suspension in water Sigma-Aldrich) was added and the resulting solution was stirred for 3 h. Tetraethyl ammonium hydroxide (TEAOH, 35 wt% solution in water Sigma-Aldrich), dipropylamine (99%, Aldrich) and cyclohexylamine (99% Sigma-Aldrich) were added and the solution was stirred for 4 days at 333 K. The solution was then transferred into a stainless-steel autoclave and held at 493 K for 24 h. Then, the autoclave was cooled down and the solid product was separated by centrifugation and washed three times with deionized water. Finally, SAPO-34 was dried and then calcined at 823 K for 5 h. The calcination heating and cooling rates were 1 and 2 K/min, respectively.

SAPO-56

SAPO-56 was synthesized employing a similar procedure reported elsewhere.[119] A gel composition of: 2.0 TMHD : 0.6 SiO_2 : 0.8 Al_2O_3 : P_2O_5: 40 H_2O was used (THMD = N,N,N tetra-methyl-hexane-1,6-diamine). In a typical synthesis, alumina was mixed

homogeneously with TMHD, orthophosphoric acid, and water. The mixture was vigorously stirred at room temperature for 6 h. After stirring, the resultant gel was transferred into a stainless steel autoclave and held at 473 K for 96 h. The SAPO-56 was recovered by centrifugation, dried overnight, and then calcined at 823 K for 6 h.

DNL-6

DNL-6 was synthesized as reported elsewhere.[116] The synthesis of DNL-6 was as follows: 1.17 g orthophosphoric acid (85 wt%) and 0.625 g tetraethyl orthosilicate were mixed with a solution of 3.06 g aluminium isopropoxide and 13.5 g deionized water. An aqueous solution of cetyltrimethylammonium bromide (CTAB) was then added followed by the addition of 1.097g of diethylamine (DEA). The solution was stirred during all the above mixing procedures. The specific gel composition for the hydrothermal synthesis was: 1 Al : 0.8 P : 0.2 Si : 1 DEA : 0.1 CTAB : 50 H_2O. The final gel mixture was transferred into a stainless-steel autoclave and held at 473 K for 24 h. After 24 h, the autoclave was cooled, the solid product collected after centrifugation, washed three times with deionized water, and dried at 373 K overnight. Calcination was carried out at 873 K for 4 h to remove organic species using heating and cooling rates of 1 and 2 K/min, respectively, to remove organic species.

APPENDIX B

CHARACTERIZATION OF CATALYSTS

XRD patterns (Figure 28) and SEM images (Figure 29) were acquired by collaborators at the Colorado School of Mines for SAPO-34, DNL-6, and SAPO-56, and are shown below.

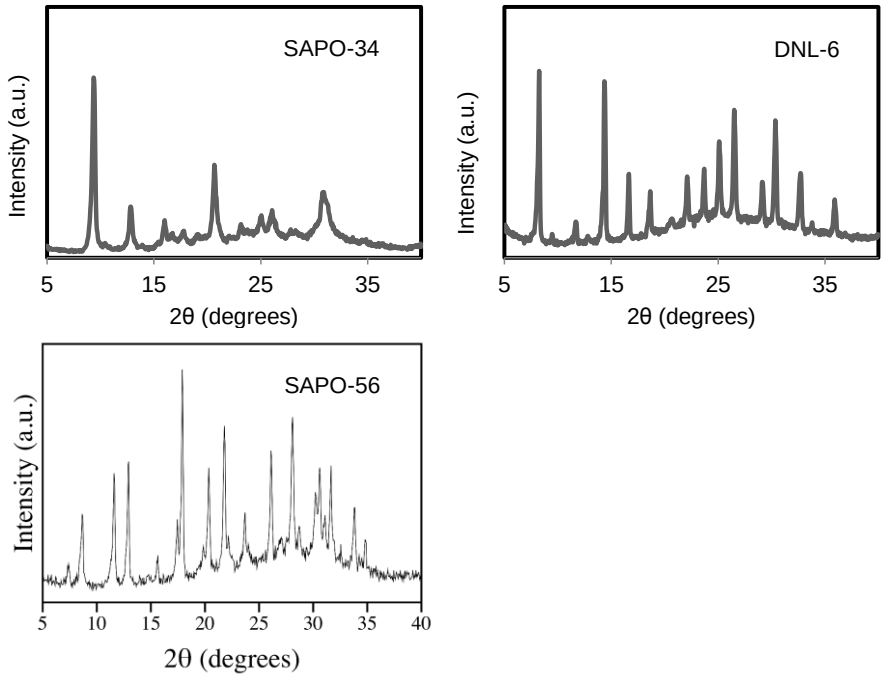

Figure 28: XRD pattern of SAPO-34, DNL-6, and SAPO-56 crystals.

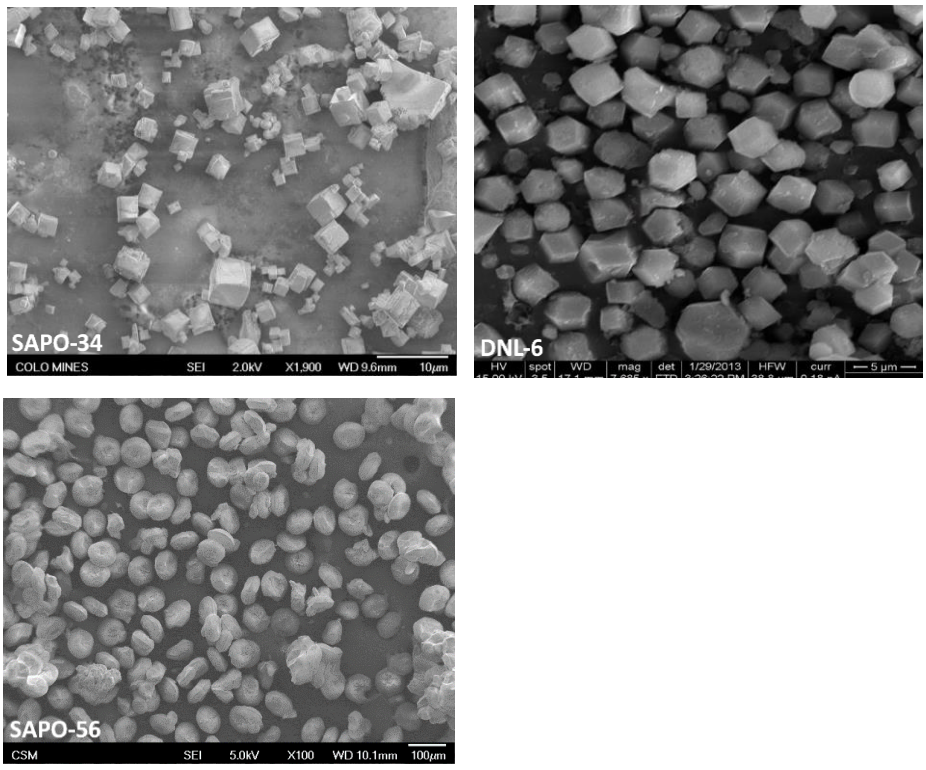

Figure 29: Representative SEM images of SAPO-34, DNL-6, and SAPO-56 crystals.

Acid site density

Brønsted and total acid site densities were determined by our collaborators at Syracuse University. The details of these measurements are given here. Brønsted site densities were determined from molar quantities of ethylene evolved between 570 K and 870 K during TPD of ethylamine. Approximately 50 mg of powdered catalyst were loaded into a quartz tube (1/2") on top of a quartz wool plug, and the tube was positioned in a high temperature furnace (Omega) and connected to a gas flow manifold. Prior to analysis, catalysts were calcined in situ at 673 K for 4 hours under 50 sccm of air (Airgas, Ultra Zero). Subsequently, the samples were cooled to 423K, and purged with 100 sccm of He that was dried over molecular sieves. After pretreatment, the samples were held at 423 K and contacted with ethylamine (99%, Sigma). Pure ethylamine was introduced into

the helium stream (100 sccm) through a 50 μm capillary tube that served to regulate the ethylamine flow. The cell was then purged with He (423 K, 100 sccm, 60 min) and subsequently ramped to 973 K (10 K min-1). During the temperature ramp, the cell effluent was monitored using a mass selective detector (Stanford Instruments RGA 100). Signals corresponding to ethylamine (m/z = 30) and ethylene (m/z = 27) were monitored continuously, and Brønsted site densities were calculated from evolved ethylene based on the assumption that one molecule of ethylene forms at one accessible Brønsted site.

Total site densities were determined from molar quantities of ammonia evolved between 423 K and 1023 K during TPD of ammonia. Approximately 50 mg of powdered catalyst were loaded into a quartz tube (1/2") on top of a quartz wool plug, and the tube was positioned in a high temperature furnace (Omega) and connected to a gas flow manifold. Prior to analysis, catalysts were calcined in situ at 673 K for 4 hours under 50 sccm of air (Airgas, Ultra Zero). Subsequently, the samples were cooled to 423 K, and purged with 100 sccm of He that was dried over molecular sieves. After pretreatment, the samples were held at 423 K and contacted with a blend of ammonia (1% ammonia in He, Airgas) until saturation. The cell was then purged with He (423 K, 100 sccm, 60 min) and subsequently ramped to 1023 K (10 K min^{-1}). During the temperature ramp, the cell effluent was monitored using a mass selective detector (Stanford Instruments RGA 100). The signal corresponding to ammonia (m/z = 16) was monitored continuously, and acid site densities were calculated from evolved ammonia, based on the assumption that one molecule of ammonia desorbs from one accessible acid site.

APPENDIX C

HPLC INSTRUMENT MAINTENANCE

Several major performance issues were encountered throughout the course of these experiments with the HPLC instrument in use, which led to a significant amount of troubleshooting and maintenance. Table 5 below shows an overview of each issue and how it was resolved.

Table 5: Summary of HPLC troubleshooting and maintenance.

Date	Symptoms of Issue	Actual Diagnosis	Resolution & Notes
October 2014	Decrease in pressure signal, increase in retention times.	Leaking capillary loop.	Replaced the leaking 100 µL capillary loop, found in the autosampler/injector unit, with a genuine Agilent replacement, p/n: 01078-87302.
November 2014	Persistent uniformly unstable pressure signal, increase in retention times.	Symptoms pointed towards worn seals in pumphead A.	Replaced the seals (2) in pumphead A with genuine Agilent replacements, p/n: 5063-6589. As a result, the pressure signal improved slightly, but was not yet back to ideal operation condition.
March 2015	Still seeing variation in pressure signal, now not always uniform as before.	Possible worn sapphire pistons in pumphead A.	Replaced the sapphire pistons (2) in pumphead A with genuine Agilent replacements, p/n: 5063-6586. As a result, the pressure signal again improved slightly, but was still not perfect.
March 2015	No UV signal.	UV lamp is likely worn out.	Replaced deuterium lamp in DAD unit, upgrading to a much newer version of the previous lamp, Agilent p/n: 5182-1530. Discussed techniques to improve lamp life with Agilent technician, who recommended shutting the lamp off only when system will be idle for greater than 24 hours.
April & May 2015	Pressure signal is still highly unstable, showing massive oscillations, both uniform and non-uniform. Issues are present on both pumpheads, A & B.	At this point, a precise diagnosis of the issue(s) is beyond our knowledge and skillset. Brought pump unit to Dr. Jonathan K. Hilmer in the MSU Mass Spectrometry Facility for help with troubleshooting.	Dr. Hilmer and his staff spent about six weeks diagnosing issues with the HPLC pump unit. They went through a significant amount of standard troubleshooting procedures, including: cleaning out active inlet valves (AIV) and check valves, cleaning other pumphead components (piston housing, etc), and running numerous leak checks across all pumphead components. They inspected various seals and other wearable components, replacing pump seals in both pumpheads (4 seals total). Still, nothing so far solved the issue. They then replaced the cartridges within the AIVs of each pumphead with genuine Agilent replacements, p/n: 5062-8562. Finally, this solved the issue and the HPLC was returned to fully functional condition.

As mentioned above in Table 5, diagnosing and fixing issues within the HPLC pumpheads was the most complex and time-consuming aspect of the HPLC troubleshooting. Pictured below in Figure 30 are the two pumpheads, both containing active inlet valves on the bottom, check valves on the top, a purge valve on pumphead A (left), and various other inlets and outlets. The cartridges within the AIV on both pumpheads were found to be the primary source of the problems with unstable and oscillatory back pressure signal; once replaced, these issues abated.

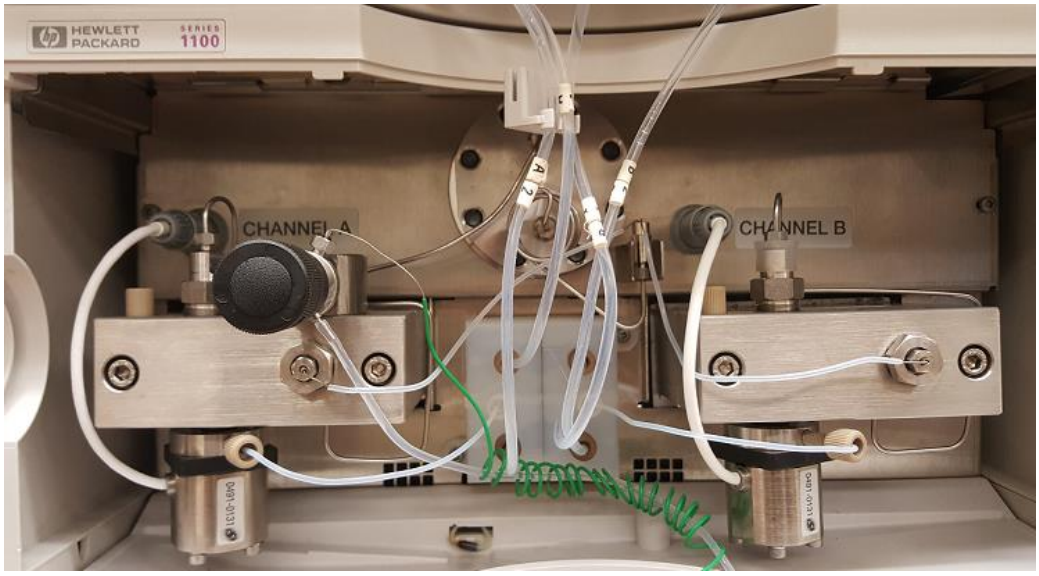

Figure 30: HPLC pumpheads A(left) and B (right).

While working with Dr. Hilmer and his staff in the MSU Mass Spectrometry Facility, ideas about systematic methods to prevent similar major instrument maintenance in the future were discussed. Their single greatest recommendation was to shift away from using 5 mM sulfuric acid as the standard running buffer, and to use formic acid or trifluoroacetic acid (TFA) instead. 5 mM sulfuric acid was initially chosen as it is the buffer that BioRad recommends for the column most commonly in use in this instrument,

a BioRad Aminex HPX-87H. After speaking with technical support staff from BioRad and with Dr. Hilmer, it was decided that either formic acid or TFA could be used with this system, provided that the buffer was prepared with a pH similar to that produced by the 5 mM sulfuric acid (pH = 2). Considering factors like chemical cost, safety, and instrument wear, a new buffer of 10 mM TFA was chosen. This is prepared by measuring 1.50 mL of TFA into 2.00 L of water via volumetric glassware, producing a new buffer with a pH = 2.016.

Because these experiments require isocratic separations, not gradient separations, only one pump (A or B) was previously being used at a time, i.e. 100% pump A or 100% pump B. It was determined that leaving either pump sitting idle for extended periods of time actually increases the wear and tear on some of its components. To combat this, a new HPLC method was created that pumps the same buffer equally on pump A and pump B (50:50) at all times. In doing so, the aim is to reduce wear on pump components typically exacerbated by pump disuse.

One final recommendation provided by Dr. Hilmer was to perform leak checks on a weekly or biweekly basis across various components of the HPLC system to catch potential issues early. To do this, he recommended ordering a blank nut (IDEX Health & Science, P-520) in order to plug the HPLC pumpheads at various locations to systematically isolate specific pump components prone to developing leaks, and find and resolve these issues before they become problematic. Leak checks can be run automatically through the Agilent Lab Adviser software.

APPENDIX D

ADDITIONAL ZSM-5 DATA

In addition to the standard reactions using 2 wt% xylose and switchgrass, a leaching study and a recyclability study were also carried out using ZSM-5 based on the methods outlined in section 3.2.5 (leaching) and section 3.3 (recyclability). The leaching study resulted in significant leaching of acid sites, with furfural yields of 52.5% and 52.4% being achieved from xylose in consecutive reactions. This indicates that a substantial number of acid sites did leach from ZSM-5, allowing the reaction to be catalyzed homogeneously. Interestingly, a leaching study with switchgrass saw zero furfural production.

Figure 31 shows the results of the recyclability study that was carried out with ZSM-5. There is a significant drop off in furfural yield from the first round of reaction (using fresh catalyst) to the second and third rounds of reaction (using spent catalyzed that was washed and baked at 573 K). Experiments were also run to ensure that baking the spent catalyst at a higher temperature (773 K) or for 72 hours at 573 K did not lead to a recovery of more catalyst activity. These other catalyst baking methods did not lead to a recovery of any catalyst activity, suggesting that coking of the catalyst is not likely to be the cause of the decreasing furfural yields. This data, coupled with the results of the leaching study, indicate that acid sites are very likely leaking from the ZSM-5 under the reaction conditions used in this project.

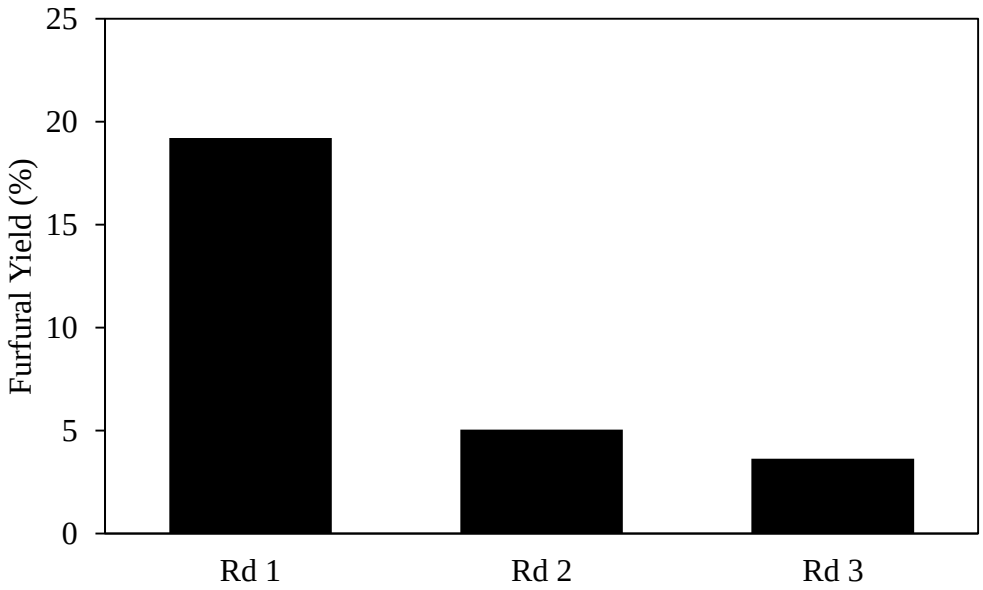

Figure 31: Recyclability study results through three rounds of reaction using ZSM-5.

REFERENCES CITED

1 Holtberg, P. *Annual Energy Outlook 2015*; United States Energy Information Administration: 2015.

2 USCG *On Scene Coordinator Report Deepwater Horizon Oil Spill*; United States Coast Guard: 2011.

3 Friberg, P. A., Besana-Ostman, G. M., and Dricker, I., *Seismological Research Letters*, 2014.

4 Heinecke, J., Jabbari, N., and Meshkati, N., *Journal of Sustainable Energy Engineering*, 2014, **2** (2), 130-151.

5 Walters, R., Zoback, M., Gupta, A., Baker, J., and Beroza, G. In *A Site Characterization Protocol for Evaluating the Potential for Triggered or Induced Seismicity Resulting from Wastewater Injection and Hydraulic Fracturing*, AGU Fall Meeting Abstracts, 2014; p 4443.

6 Rosenzweig, C., Karoly, D., Vicarelli, M., Neofotis, P., Wu, Q., Casassa, G., Menzel, A., Root, T. L., Estrella, N., Seguin, B., Tryjanowski, P., Liu, C., Rawlins, S., and Imeson, A., *Nature*, 2008, **453** (7193), 353-357.

7 Sahu, R., and Dhepe, P. L., *Chemsuschem*, 2012, **5** (4), 751-761.

8 L.T. Fan, M. M. G., Y.H. Lee, in *Cellulose Hydrolysis*. Berling, Germany, Springer-Verlag, 1987.

9 Perlack, R. D., Wright, L. L., Turhollow, A. F., Graham, R. L., Stokes, B. J., and Erbach, D. C. *Biomass as feedstock for a bioenergy and bioproducts industry: the technical feasibility of a billion-ton annual supply*; DTIC Document: 2005.

10 Nations, U. *The State of Food Insecurity in the World*; 2014.

11 Gallezot, P., *Chem. Soc. Rev.*, 2012, **41** (4), 1538-1558.

12 McKendry, P., *Bioresour. Technol.*, 2002, **83** (1), 37-46.

13 Gibson, L. J., *Journal of the Royal Society Interface*, 2012, rsif20120341.

14 Klemm, D., Heublein, B., Fink, H.-P., and Bohn, A., *Angewandte Chemie International Edition*, 2005, **44** (22), 3358-3393.

15 Scheller, H. V., and Ulvskov, P., *Annual Review of Plant Biology*, 2010, **61** (1), 263-289.

16 Lebo, S. E., Gargulak, J. D., and McNally, T. J., Lignin. In *Kirk-Othmer Encyclopedia of Chemical Technology*, John Wiley & Sons, Inc., 2000.

17 *US Pat.*, US8372165-B1.

18 Lange, J. P., van der Heide, E., van Buijtenen, J., and Price, R., *Chemsuschem*, 2012, **5** (1), 150-166.

19 Gurbuz, E. I., Gallo, J. M. R., Alonso, D. M., Wettstein, S. G., Lim, W. Y., and Dumesic, J. A., *Angew. Chem., Int. Ed.*, 2013, **52** (4), 1270-1274.

20 Choudhary, V., Sandler, S. I., and Vlachos, D. G., *Acs Catalysis*, 2012, **2** (9), 2022-2028.

21 Peters Jr, F. N., *Industrial & Engineering Chemistry*, 1939, **31** (2), 178-180.

22 Dias, A. S., Lima, S., Pillinger, M., and Valente, A. A., *Ideas in Chemistry and Molecular Sciences: Advances in Synthetic Chemistry*, 2010, **8**, 167-186.

23 Win, D. T., *Au J Technol*, 2005, **8**, 185-190.

24 Yan, K., Wu, G., Lafleur, T., and Jarvis, C., *Renewable and Sustainable Energy Reviews*, 2014, **38** (0), 663-676.

25 Zeitsch, K. J., in *The chemistry and technology of furfural and its many by-products*. Elsevier, 2000; Vol. 13.

26 Yebo, D. Furfural Market Prices. http://www.dalinyebo.com/item/770-furfural-market-prices-2014.

27 Montastruc, L., Ajao, O., Marinova, M., Do Carmo, C. B., and Domenech, S., *Cellulose*, 2011, **3** (6.54).

28 Tuskan, G., *Biomass and Bioenergy*, 1998, **14** (4), 307-315.

29 McLaughlin, S. B., and Adams Kszos, L., *Biomass and Bioenergy*, 2005, **28** (6), 515-535.

30 Sanderson, M., Reed, R., McLaughlin, S., Wullschleger, S., Conger, B., Parrish, D., Wolf, D., Taliaferro, C., Hopkins, A., and Ocumpaugh, W., *Bioresource Technology*, 1996, **56** (1), 83-93.

31 McLaughlin, S. *New switchgrass biofuels research program for the southeast*; Oak Ridge National Lab., TN (United States): 1992.

32 USDA, N., Plant Fact Sheet, Panicum virgatum (Switchgrass). 2006.

33 Lee, D., and Initiative, S. G., in *Composition of herbaceous biomass feedstocks*. North Central Sun Grant Center, South Dakota State University, 2007.

34 Ma, F., and Hanna, M. A., *Bioresource Technology*, 1999, **70** (1), 1-15.

35 Farrell, A. E., Plevin, R. J., Turner, B. T., Jones, A. D., O'hare, M., and Kammen, D. M., *Science*, 2006, **311** (5760), 506-508.

36 Chum, H. L., Warner, E., Seabra, J. E. A., and Macedo, I. C., *Biofuels, Bioproducts and Biorefining*, 2014, **8** (2), 205-223.

37 Naik, S. N., Goud, V. V., Rout, P. K., and Dalai, A. K., *Renewable and Sustainable Energy Reviews*, 2010, **14** (2), 578-597.

38 Fernando, S., Adhikari, S., Chandrapal, C., and Murali, N., *Energy & Fuels*, 2006, **20** (4), 1727-1737.

39 Dellomonaco, C., Fava, F., and Gonzalez, R., *Microb Cell Fact*, 2010, **9** (3), 1-15.

40 Williams, P. R., Inman, D., Aden, A., and Heath, G. A., *Environmental science & technology*, 2009, **43** (13), 4763-4775.

41 Bajhaiya, A., Mandotra, S., Suseela, M., Toppo, K., and Ranade, S., *Asian J. Exp. Biol. Sci*, 2010, **4**, 728-739.

42 Simmons, B. A., Loque, D., and Blanch, H. W., *Genome biology*, 2008, **9** (2), 242-242.

43 Zinoviev, S., Müller-Langer, F., Das, P., Bertero, N., Fornasiero, P., Kaltschmitt, M., Centi, G., and Miertus, S., *Chemsuschem*, 2010, **3** (10), 1106-1133.

44 Lu, Y., and Mosier, N. S., *Biotechnol. Prog.*, 2007, **23** (1), 116-123.

45 Danner, H., and Braun, R., *Chem. Soc. Rev.*, 1999, **28** (6), 395-405.

46 Jensen, J. R., Morinelly, J. E., Gossen, K. R., Brodeur-Campbell, M. J., and Shonnard, D. R., *Bioresour. Technol.*, 2010, **101** (7), 2317-2325.

47 Wyman, C. E., Dale, B. E., Elander, R. T., Holtzapple, M., Ladisch, M. R., and Lee, Y. Y., *Bioresour. Technol.*, 2005, **96**, 2026 - 2032.

48 Geboers, J., Van de Vyver, S., Carpentier, K., Jacobs, P., and Sels, B., *Chemical Communications*, 2011, **47** (19), 5590-5592.

49 Maki-Arvela, P., Salmi, T., Holmbom, B., Willfor, S., and Murzin, D. Y., *Chem. Rev.*, 2011, **111** (9), 5638-5666.

50 Gallo, J. M. R., Alonso, D. M., Mellmer, M. A., Yeap, J. H., Wong, H. C., and Dumesic, J. A., *Topics in Catalysis*, 2013, **56** (18-20), 1775-1781.

51 Wettstein, S. G., Alonso, D. M., Chong, Y. X., and Dumesic, J. A., *Energy Environ. Sci.*, 2012, **5** (8), 8199-8203.

52 Yamaguchi, D., Kitano, M., Suganuma, S., Nakajima, K., Kato, H., and Hara, M., *Journal of Physical Chemistry C*, 2009, **113** (8), 3181-3188.

53 Lai, D.-m., Deng, L., Guo, Q.-x., and Fu, Y., *Energy Environ. Sci.*, 2011, **4** (9), 3552-3557.

54 Van de Vyver, S., Peng, L., Geboers, J., Schepers, H., de Clippel, F., Gommes, C. J., Goderis, B., Jacobs, P. A., and Sels, B. F., *Green Chem.*, 2010, **12** (9), 1560-1563.

55 Katiyar, A., Yadav, S., Smirniotis, P. G., and Pinto, N. G., *Journal of Chromatography A*, 2006, **1122** (1–2), 13-20.

56 Vincent, C., Process for producing low-bulk density silica. Google Patents, 1971.

57 Di Renzo, F., Cambon, H., and Dutartre, R., *Microporous Materials*, 1997, **10** (4–6), 283-286.

58 Nandiyanto, A. B. D., Iskandar, F., and Okuyama, K., *Chemistry Letters*, 2008, **37** (10), 1040-1041.

59 Nandiyanto, A. B. D., Kim, S.-G., Iskandar, F., and Okuyama, K., *Microporous and Mesoporous Materials*, 2009, **120** (3), 447-453.

60 Trewyn, B. G., Nieweg, J. A., Zhao, Y., and Lin, V. S. Y., *Chemical Engineering Journal*, 2008, **137** (1), 23-29.

61 Radu, D. R., Lai, C.-Y., Jeftinija, K., Rowe, E. W., Jeftinija, S., and Lin, V. S. Y., *Journal of the American Chemical Society*, 2004, **126** (41), 13216-13217.

62 Mellaerts, R., Aerts, C. A., Humbeeck, J. V., Augustijns, P., den Mooter, G. V., and Martens, J. A., *Chemical Communications*, 2007, (13), 1375-1377.

63 Kleitz, F. Ordered Nanoporous Materials: Synthesis, Characterization and Functionalization Methods.

64 Shi, X., Wu, Y., Yi, H., Rui, G., Li, P., Yang, M., and Wang, G., *Energies*, 2011.

65 Dias, A. S., Pillinger, M., and Valente, A. A., *Journal of Catalysis*, 2005, **229** (2), 414-423.

66 Dias, A. S., Pillinger, M., and Valente, A. A., *Microporous and Mesoporous Materials*, 2006, **94** (1–3), 214-225.

67 Xie, Z. K., Liu, Z. C., Wang, Y. D., Yang, Q. H., Xu, L. Y., and Ding, W. P., *International Journal of Molecular Sciences*, 2010, **11** (5), 2152-2187.

68 de Dardel, F., and Arden, T. V., Ion Exchangers. In *Ullmann's Encyclopedia of Industrial Chemistry*, Wiley-VCH Verlag GmbH & Co. KGaA, 2000.

69 Arden, T. V., in *Water purification by ion exchange*. Springer Science & Business Media, 2012.

70 Berdous, D., and Akretche, D., *Desalination*, 2002, **144** (1), 213-218.

71 Small, H., Stevens, T. S., and Bauman, W. C., *Analytical Chemistry*, 1975, **47** (11), 1801-1809.

72 Chakrabarti, A., and Sharma, M., *Reactive Polymers*, 1993, **20** (1), 1-45.

73 Harmer, M. A., and Sun, Q., *Applied Catalysis A: General*, 2001, **221** (1), 45-62.

74 Alonso, D. M., Gallo, J. M. R., Mellmer, M. A., Wettstein, S. G., and Dumesic, J. A., *Catal. Sci. Technol.*, 2013, **3** (4), 927-931.

75 Carà, P. D., Pagliaro, M., Elmekawy, A., Brown, D. R., Verschuren, P., Shiju, N. R., and Rothenberg, G., *Catal. Sci. Technol.*, 2013, **3** (8), 2057-2061.

76 Antunes, M. M., Lima, S., Fernandes, A., Pillinger, M., Ribeiro, M. F., and Valente, A. A., *Appl. Catal., A*, 2012, **417**, 243-252.

77 Sjoman, E., Manttari, M., Nystrom, M., Koivikko, H., and Heikkila, H., *Journal of Membrane Science*, 2007, **292** (1-2), 106-115.

78 Jae, J., Tompsett, G. A., Foster, A. J., Hammond, K. D., Auerbach, S. M., Lobo, R. F., and Huber, G. W., *Journal of Catalysis*, 2011, **279** (2), 257-268.

79 Wettstein, S. G., Alonso, D. M., Gürbüz, E. I., and Dumesic, J. A., *Curr. Opin. Chem. Eng.*, 2012, **1** (3), 218-224.

80 Nikolla, E., Roman-Leshkov, Y., Moliner, M., and Davis, M. E., *ACS Catal.*, 2011, **1** (4), 408-410.

81 Lei, X.-g., Jockusch, S., Francesca Ottaviani, M., and Turro, N. J., *Photochemical & Photobiological Sciences*, 2003, **2** (11), 1095-1100.

82 Moreau, C., Durand, R., Peyron, D., Duhamet, J., and Rivalier, P., *Ind. Crops Prod.*, 1998, **7** (2-3), 95-99.

83 Lima, S., Antunes, M. M., Fernandes, A., Pillinger, M., Ribeiro, M. F., and Valente, A. A., *Appl. Catal., A*, 2010, **388** (1-2), 141-148.

84 Lourvanij, K., and Rorrer, G. L., *Ind. Eng. Chem. Res.*, 1993, **32** (1), 11-19.

85 O'Neill, R., Ahmad, M. N., Vanoye, L., and Aiouache, F., *Ind. Eng. Chem. Res.*, 2009, **48** (9), 4300-4306.

86 Kim, S. B., You, S. J., Kim, Y. T., Lee, S., Lee, H., Park, K., and Park, E. D., *Korean Journal of Chemical Engineering*, 2011, **28** (3), 710-716.

87 Weitkamp, J., *Solid State Ionics*, 2000, **131** (1–2), 175-188.

88 Hartley, O., Method for catalytic cracking of residual oils. Google Patents, 1975.

89 Naber, J., De Jong, K., Stork, W., Kuipers, H., and Post, M., *Studies in surface science and catalysis*, 1994, **84**, 2197-2219.

90 Kulprathipanja, S., in *Zeolites in industrial separation and catalysis*. John Wiley & Sons, 2010.

91 IZA Gismondine. http://www.iza-online.org/natural/Datasheets/Gismondine/gismondine.htm.

92 Minerals, D. M. Chabazite. http://www.dakotamatrix.com/products/1885/chabazite.

93 IZA Chabazite. http://www.iza-online.org/natural/Datasheets/Chabazite/chabazite.htm.

94 Seaterror Synthetic Zeolite. https://commons.wikimedia.org/wiki/File:Ceolite_nax.JPG.

95 Weingarten, R., Tompsett, G. A., Conner, W. C., Jr., and Huber, G. W., *Journal of Catalysis*, 2011, **279** (1), 174-182.

96 Ward, J. W., *Journal of Catalysis*, 1967, **9** (3), 225-236.

97 Coster, D., Blumenfeld, A. L., and Fripiat, J. J., *The Journal of Physical Chemistry*, 1994, **98** (24), 6201-6211.

98 Poduval, D. G., Van Veen, J. R., Rigutto, M. S., and Hensen, E. J., *Chemical Communications*, 2010, **46** (20), 3466-3468.

99 Huang, J., Jiang, Y., Marthala, V. R., Thomas, B., Romanova, E., and Hunger, M., *The Journal of Physical Chemistry C*, 2008, **112** (10), 3811-3818.

100 Reddy, C. R., Bhat, Y., Nagendrappa, G., and Prakash, B. J., *Catalysis Today*, 2009, **141** (1), 157-160.

101 Yang, Y.-l., and Kou, Y., *Chemical Communications*, 2004, (2), 226-227.

102 Firoozi, M., Baghalha, M., and Asadi, M., *Catalysis Communications*, 2009, **10** (12), 1582-1585.

103 Foster, A. J., Jae, J., Cheng, Y.-T., Huber, G. W., and Lobo, R. F., *Applied Catalysis A: General*, 2012, **423–424** (0), 154-161.

104 Corbin, D. R., Fagan, P. J., Fergusson, S. B., Hutchenson, K. W., Metkar, P. S., Ozer, R., Pereira, C. J., Rajagopalan, B., Sengupta, S. K., and Till, E. J., Process for the production of furfural. Google Patents, 2015.

105 Conner, W. C., Vincent, R., Man, P., and Fraissard, J., *Catal. Lett.*, 1990, **4** (1), 75-83.

106 Baimpos, T., Kouzoudis, D., Gora, L., and Nikolakis, V., *Chem. Mater.*, 2011, **23** (6), 1347-1349.

107 Sorenson, S. G., Payzant, E. A., Noble, R. D., and Falconer, J. L., *J. Membr. Sci.*, 2010, **357**, 98-104.

108 Yu, M., Li, S. G., Falconer, J. L., and Noble, R. D., *Microporous Mesoporous Mater.*, 2008, **110** (2-3), 579-582.

109 Hammonds, K. D., Heine, V., and Dove, M. T., *J. Phys. Chem. B*, 1998, **102** (10), 1759-1767.

110 Sartbaeva, A., Wells, S. A., Treacy, M. M. J., and Thorpe, M. F., *Nat. Mater.*, 2006, **5** (12), 962-965.

111 Cox, D. M., High surface area materials. In *Nanostructure Science and Technology*, Springer, 1999; pp 49-66.

112 Lok, B. M., Messina, C. A., Patton, R. L., Gajek, R. T., Cannan, T. R., and Flanigen, E. M., *Journal of the American Chemical Society*, 1984, **106** (20), 6092-6093.

113 Szostak, R., in *Handbook Of Molecular Sieves: Structures*. Springer Science & Business Media, 1992.

114 Su, X., Tian, P., Li, J. Z., Zhang, Y., Meng, S. H., He, Y. L., Fan, D., and Liu, Z. M., *Microporous and Mesoporous Materials*, 2011, **144** (1-3), 113-119.

115 Harris, D. C., in *Quantitative chemical analysis*. Macmillan, 2010.

116 Su, X., Tian, P., Li, J., Zhang, Y., Meng, S., He, Y., Fan, D., and Liu, Z., *Microporous and Mesoporous Materials*, 2011, **144** (1-3), 113-119.

117 Venna, S. R., and Carreon, M. A., *Chemical Engineering Science*, 2015, **124** (0), 3-19.

118 Carreon, M. A., Li, S., Falconer, J. L., and Noble, R. D., *Advanced Materials*, 2008, **20** (4), 729-732.

119 Wilson, S. T., Broach, R. W., Blackwell, C. S., Bateman, C. A., McGuire, N. K., and Kirchner, R. M., *Microporous and Mesoporous Materials*, 1999, **28** (1), 125-137.

120 IZA Framework Type CHA. http://izasc-mirror.la.asu.edu/fmi/xsl/IZA-SC/Atlas_pdf/CHA.pdf.

121 Xie, Z., Zhu, M., Nambo, A., Jasinski, J. B., and Carreon, M. A., *Dalton Trans.*, 2013, **42** (19), 6732-6735.

122 IZA Framework Type AFX. http://izasc-mirror.la.asu.edu/fmi/xsl/IZA-SC/Atlas_pdf/AFX.pdf.

123 Su, X., Tian, P., Li, J. Z., Zhang, Y., Meng, S. H., He, Y. L., Fan, D., and Liu, Z. M., *Microporous Mesoporous Mater.*, 2011, **144** (1-3), 113-119.

124 IZA Framework Type Rho. http://izasc-mirror.la.asu.edu/fmi/xsl/IZA-SC/Atlas_pdf/RHO.pdf.

125 IZA, 1978.

126 Bicker, M., Hirth, J., and Vogel, H., *Green Chem.*, 2003, **5** (2), 280-284.

127 Jin, F., and Enomoto, H., *Energy Environ. Sci.*, 2011, **4** (2), 382-397.

128 Gurbuz, E. I., Gallo, J. M., Alonso, D. M., Wettstein, S. G., Lim, W. Y., and Dumesic, J. A., *Angew. Chem. Int. Ed.*, 2013, **52** (4), 1270-1274.

129 Mellmer, M. A., Sener, C., Gallo, J. M. R., Luterbacher, J. S., Alonso, D. M., and Dumesic, J. A., *Angew. Chem., Int. Ed.*, 2014, **53** (44), 11872-11875.

130 Akiya, N., and Savage, P. E., *Chem. Rev.*, 2002, **102** (8), 2725-2750.

131 Lam, E., Chong, J. H., Majid, E., Liu, Y., Hrapovic, S., Leung, A. C. W., and Luong, J. H. T., *Carbon*, 2012, **50** (3), 1033-1043.

132 Suprun, W., Lutecki, M., Haber, T., and Papp, H., *J. Mol. Catal. A: Chem.*, 2009, **309** (1–2), 71-78.

133 Choudhary, V., Mushrif, S. H., Ho, C., Anderko, A., Nikolakis, V., Marinkovic, N. S., Frenkel, A. I., Sandler, S. I., and Vlachos, D. G., *Journal of the American Chemical Society*, 2013, **135** (10), 3997-4006.

134 Grinsted, R. A., Jen, H. W., Montreuil, C. N., Rokosz, M. J., and Shelef, M., *Zeolites*, 1993, **13** (8), 602-606.

135 Fickel, D. W., D'Addio, E., Lauterbach, J. A., and Lobo, R. F., *Applied Catalysis B: Environmental*, 2011, **102** (3–4), 441-448.

136 Moliner, M., Franch, C., Palomares, E., Grill, M., and Corma, A., *Chemical Communications*, 2012, **48** (66), 8264-8266.

137 Ye, Q., Wang, L., and Yang, R. T., *Applied Catalysis A: General*, 2012, **427–428** (0), 24-34.

138 Wilson, S., and Barger, P., *Microporous and Mesoporous Materials*, 1999, **29** (1–2), 117-126.

139 Fernandez, C., Stan, I., Gilson, J. P., Thomas, K., Vicente, A., Bonilla, A., and Pérez-Ramírez, J., *Chemistry-A European Journal*, 2010, **16** (21), 6224-6233.

140 Gounder, R., and Iglesia, E., *Journal of the American Chemical Society*, 2009, **131** (5), 1958-1971.

141 Corma, A., *Journal of Catalysis*, 2003, **216** (1–2), 298-312.